

HALTERES AND CONTROL OF FLIGHT IN DIPTERANS

A STUDY IN FREE FLIGHT

A THESIS SUBMITTED
FOR THE COMPLETION OF THE DEGREE
BACHELOR OF SCIENCE
(RESEARCH)

by
ADITYA ANANTHANARAYANAN IYER
Undergraduate Programme
Indian Institute of Science



supervised by

PROF. ROHINI BALAKRISHNAN

Centre for Ecological Sciences
Institute of Indian Science

PROF. SANJAY SANE

National Center for Biological Sciences

ABSTRACT

Halteres are specialised mechanosensory organs, characteristic to Dipterans that sense rotational perturbations in flight and provide feedback for maintaining flight control. The mechanism of how these vibrating gyroscopic organs aid in flight control has been an active subject of interest for the past century. Several strides towards understanding the role of halteres in flight have been made, from detailed theoretical considerations, to morphological and neuroanatomical descriptions of haltere efferents. High speed videography has facilitated significant advances by allowing finer observations of flight. Behavioural studies using tethered Dipterans have provided insight into the possible effects of haltere inputs on flight. In this study, the changes in wing kinetic parameters of unilateral and bilateral ablation of halteres have been compared in the soldier fly, *Hermetia illucens* as it freely flies in a closed chamber.

The first 200-350 ms of flight in *H. illucens* has been filmed in a custom behavioural rig, using 3 orthogonally placed high speed cameras at 2800 fps. Three experimental treatment groups of soldier flies were used: right haltere ablated, left haltere ablated and a control with no ablation.

A deep learning tool, DeepLabCut has been used for automatically obtaining pixel coordinates of relevant points of a fly from collected videos, as opposed to the time consuming traditional method of manually labelling each frame in a video. I have interfaced this tool with DLTdv7, a more popular manual digitization tool to increase accuracy and reduce computational requirements of DeepLabCut.

Our collected data in free flight supports published tethered flight experiments in *Drosophila*, suggesting that haltere ablation inhibits ipsilateral wing kinematics. Unlike the housefly *Musca*, *H. illucens* don't show handedness in roll rotations on haltere ablation. Most likely, this is due to the slower wing beat frequency of soldier flies, allowing visual input integration for maintaining better control in flight.

ACKNOWLEDGEMENTS

I must thank the following people for their role in this project:

- My mentor, Prof. Sanjay Sane (NCBS) for hosting me in his lab, and providing valuable inputs and feedback which drove the course of this project.
- Prof. Rohini Balakrishnan (CES, IISc) for valuable feedback on the structure and content of this thesis
- My lab mates for insightful discussions and a welcoming lab environment
- Maitri M and Abin Ghosh for teaching me the handling and use of high speed cameras.
- Dinesh Natesan for his MATLAB scripts
- Mr. Kemperaju M for managing the soldier fly cultures.

Finally, I thank the DST for its KVPY scholarship, which funded me through my education at IISc, Bengaluru.

CERTIFICATE

Mr Aditya Ananthanarayanan Iyer has worked under my supervision between October 2018 and April 2019. I have gone through his work on the role of halteres in the control of Dipteran flight presented in this thesis, and have found it to be satisfactory.

Prof. Rohini Balakrishnan

Centre for Ecological Sciences

Indian Institute of Science

Prof. Sanjay Sane

National Center for Biological Sciences

Tata Institute of Fundamental Research

DECLARATION

I, Aditya Ananthanarayanan Iyer, have under the supervision of Prof Sanjay Sane (NCBS) and Prof Rohini Balakrishnan (CES, IISc) between October 2018 and April 2019, participated in a project to investigate the role of halteres in the control of Dipteran flight. No unfair means have been used at any point in this project.

Aditya Ananthanarayanan Iyer
Undergraduate Programme (Biology)
Indian Institute of Science

CONTENTS

1	Introduction	1
1.1	Control of Flight	1
1.2	Halteres	4
1.3	Research Question and Motivation	11
1.4	References	14
2	Methods	17
2.1	Soldier fly Rearing and Collection	17
2.2	Haltere Ablation	18
2.3	High Speed Filming	18
2.4	Flight Initiation Paradigm	23
2.5	Digitization	25
2.6	References	33
3	Analysis and Results	34
3.1	Analysis	34
3.2	Results	38
4	Discussion	46
4.1	Haltere Ablated Flies Pitch Up	46
4.2	Right Haltere Ablated Flies Have Higher Roll Velocities	46
4.3	Ventral Excursion maxima in stroke angle is reduced on Haltere Ablation	47
4.4	Comparisons with free flight in haltere ablated <i>Musca</i>	47
4.5	Digitization and DeepLabCut	51
4.6	Future Directions	52
4.7	References	54

LIST OF FIGURES

1	Rotational Axes	2
2	Wing Kinematics (Dickinson et al. 2016)	3
3	Campaniform sensilla fields (Yarger, 2016)	8
4	Neural Circuitry (Lehmann and Bartussek 2017)	10
5	Control Theory Models (Dickinson 2016)	11
6	Soldier fly <i>H. illucens</i>	13
7	<i>H. illucens</i> Halteres	13
8	Halteres ablated at the base	18
9	Higher sampling rate for better estimation	19
10	Direct Linear Transform	21
11	Direct Linear Transform Matrix	22
12	Flight Chamber Setup	24
13	DeepLabCut labeled frames	30
14	DLTdv7 GUI	31
15	Digitization Protocol	32
16	Vectors Defining Rotations in Free Flight	35
17	Filtering Deviation Angles Preserves Peaks	36
18	Wing Angle Time Evolution	36
19	Body Angle Time Course	38
20	Comparing Angular Velocities along rotational axes	39
21	Comparing Mean Rotational Angles	40
22	Comparing Stroke Angles Across Treatments	41
23	Comparing Wing-Wing Stroke Angle Differences Across Treatments	43

24	Comparing Deviation Angles Across Treatments	44
25	Comparing Wing-Wing Deviation Angle Differences Across Treatments	45
26	Musca Angular Rotation Time Evolution	48
27	Musca Wing Parameters	49

CHAPTER 1

INTRODUCTION

A flying insect is subject to many perturbations such as gusts of wind, a sudden predatory strike or an approaching obstacle in its flight path. To maintain stable flight, the fly must be able to rapidly sense these perturbations using any sensory modalities, process them and make the appropriate adjustments to its flight path. These responses occur in timescales that are very fast, and in many cases the latency from stimulus to response occurs in time scales of a few milliseconds. Insect flight behaviour is thus an epitome of multisensory integration, with fast computations and outputs.

The mechanisms mediating these precise and rapid flight responses have puzzled researchers for more than a century. Researchers have made several strides towards understanding the aerodynamics of flapping flight, the muscle morphology underlying wing movements, the sensory modalities required for sensing self-motion in flight and the sensory-motor neural circuitry for flight. In addition to neuroanatomical tools and microscopy, the development of high-speed videography has also facilitated significant advances by allowing a closer look at flight behaviour.

In this chapter, I will briefly review the research on control of flight in Dipteran insects and mechanosensory inputs aiding in flight control, specifically, the rotation-sensing halteres.

1.1 CONTROL OF FLIGHT

To determine flight control parameters, it is first necessary to establish an appropriate coordinate system. In the fly's frame of reference, three axes can be used to classify flight maneuvers: pitch, roll and yaw. These are essentially the same as their airplane counterparts.

If a fly is placed at the origin of a Cartesian coordinate axis, along the positive X axis, the X axis is the roll axis, Y axis the pitch axis, and Z axis the yaw axis (Figure 1). Wing kinematics can be described by three Euler angles - the wing stroke angle, deviation angle and wing rotation angle - with reference to the stroke plane. The deviation angle is the polar angle to the stroke plane of the vector joining the wing-base to the wing-tip. The stroke angle is the azimuthal angle of this vector in the stroke plane. The rotation angle characterises the twist of the wing (Dickinson et al. 2016).

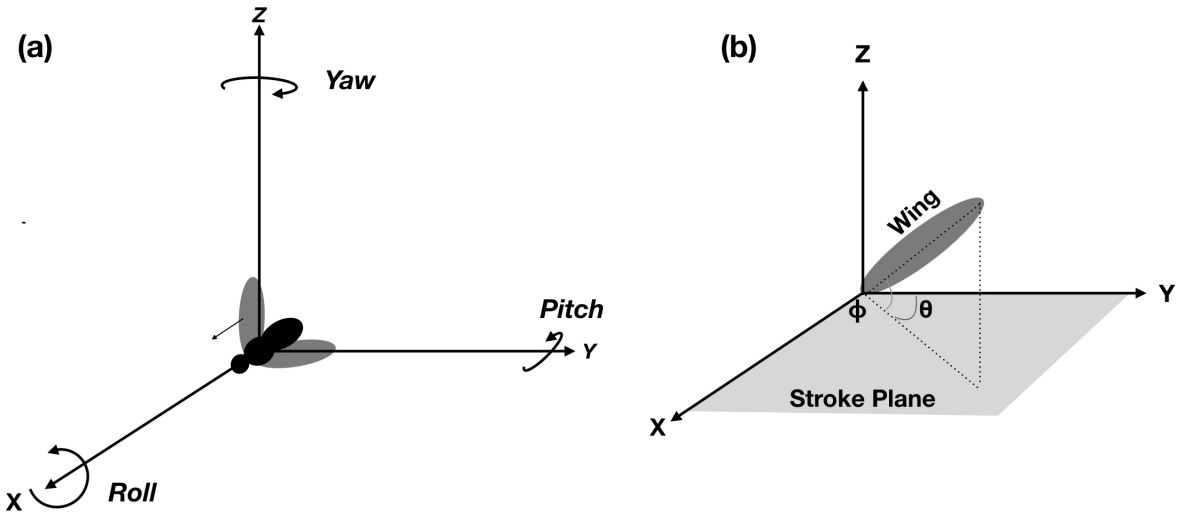


FIGURE 1: (a): Rotational Axes for Flight (b): Wing Kinetic Parameters. θ Stroke Angle, ϕ Deviation Angle

Wing movements are divided into a forward (dorsal to ventral) and a reverse (ventral to dorsal) stroke. In flying insects, the wing has a positive angle of attack on each stroke, and this generates an upward lift force in both strokes. Stability of flight is mediated by the control of torques around the body by controlling wing kinematics, whereas forward thrust is typically controlled by adjusting the body angle, similar to a helicopter.

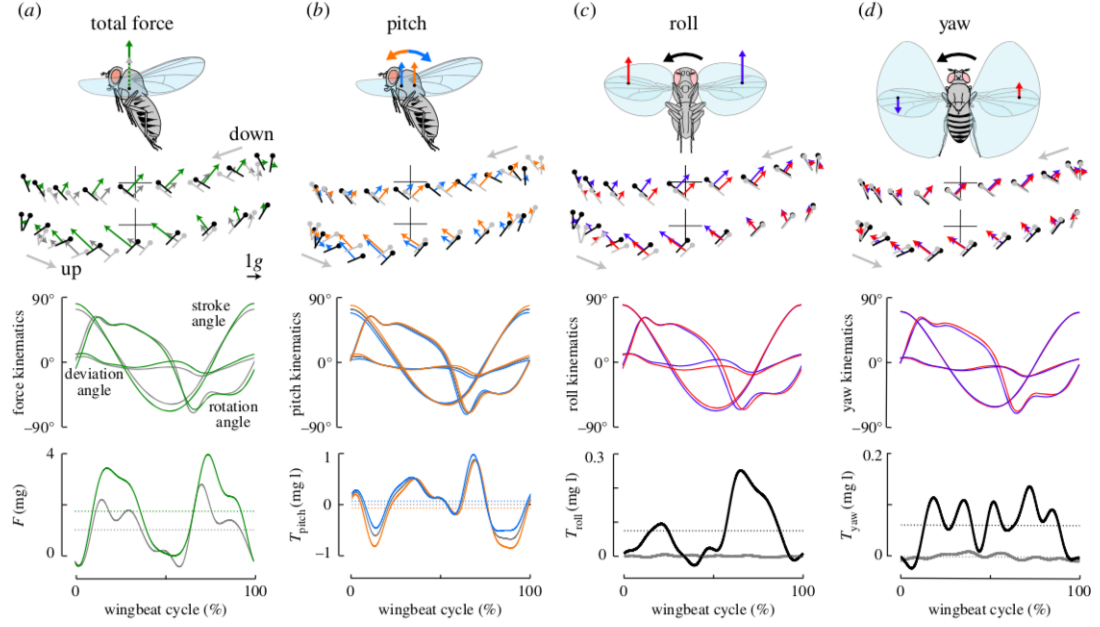


FIGURE 2: : Torque along the coordinate axes can be modulated by wing kinetic parameters.
 (a) Kinematics in stable flight. (b) Pitch: (c) Roll: Asymmetric wingstroke amplitude (d)
 Yaw: Asymmetric Wing rotation angles (From Dickinson et al. 2016)

Pitch torques are modulated by changing the time course of the stroke angles. Depending on the pitch requirement, the dorsal excursion of the wing shifts forward or backward. Roll torques are modulated mainly by the wing stroke amplitudes. A fly can increase stroke amplitude, advance wing rotation and elevate the deviation of one wing, while performing the opposite in the other wing to produce appropriate roll torques. Yaw torques are modulated almost exclusively by the wing rotation angle. Changing the wing rotation of one wing with respect to the other, and alternating the rotation in alternate half strokes of the wing changes the angle of attack between the wings. This differential creates a net yaw torque. (Dickinson et al. 2016) (Figure 2)

Wing movements in insects are powered by flight muscles in the thorax. In general, there are two types of flight muscle arrangements: the direct flight muscles (DFMs) and the Indirect flight muscles (IFMs). In DFMs, which occur in certain insects such as Odonates (e.g. *Damselflies*) and Ephemeroptera(e.g. *Mayflies*), muscles attach directly to the wing base. In contrast, for most Neopteran insects, the muscles attach to the thorax. In these insects, wing oscillations are mediated by thoracic oscillations. Moreover, in certain insects such as Diptera (e.g. *Drosophila*), Coleoptera (Beetles) and Hymenoptera (e.g. *Wasps*), the IFMs possess a

property of delayed stretch-activation; these muscles generate forces with some delay whenever they are stretched, rather than by neural activation. When set up in an antagonistic arrangement within the thorax, these muscles oscillate the thoracic cavity, and actuate the reciprocal movements of the wings (Deora et al. 2017). Specifically, in blowflies, the large IFMs provide mechanical power to move the wings through a complex linkage system at the wing hinge (Dickinson and Tu, 1997; Deora et al. 2015). In addition to these power muscles, there are 18 pairs of smaller steering muscles which receive precisely timed activation during rapid maneuvers to mediate fine control of these wing kinetic parameters (Dickinson and Tu 1997).

To maintain control, flies require constant sensory feedback about flight and the environment. At wing stroke frequencies of the order of 10^2 Hz, the timescales associated with each wingbeat are on the order of 10 ms. The latency of response at the thoracic flight muscles for visual inputs is around 25-30 ms in *Drosophila* (Sherman and Dickinson 2003). Hence, flies cannot rely on visual inputs alone for stable control of flight.

Flies instead rely on mechanosensory feedback, which generally have lower response latencies (Sherman and Dickinson 2006). Flying insects generally obtain mechanosensory feedback through antennae and sensory fields on wings. In the insect order of Diptera, the hindwings have evolved into specialised mechanosensory organs called halteres.

1.2 HALTERES

First recorded in 1714 by W. Derham in a footnote in his treatise on the *workings of the creations of God*, it was noted that if one of the two auxiliary wings (or 'poisses', as he termed them) is removed, the fly would fly to one side, as if overbalanced, and if both were removed, the fly would fly 'awkwardly and unsteadily'. He suggested that the auxiliary wings help maintain stability of the body of the fly during flight, against all perturbations (Derham, 1714), akin to a pole while walking on a tight-rope. These auxiliary wings were later renamed as halteres, after the Greek word for dumbbells, owing to their shape. Halteres have an asymmetric bulb attached to a slender stalk and are a characteristic of the insect order Diptera. The end-bulb

is filled with highly vacuolar cells which keep it distended, due to turgor pressure. The lengths of the haltere stalks differ across Dipteran classes. In insects with very small stalks, halteres are shielded by a cap, likely preventing extraneous disturbance (Pringle, 1948).

Phylogenetic comparisons with other insect orders indicate that halteres are highly modified hindwings. They emerge from the metathorax, which house the hindwing in most other orders of Insecta. Downregulation of the patterning gene (Ubx) responsible for the development of the forewing and haltere in *Drosophila*, leads to a homeotic transformation of the halteres into hind-wings, supporting the theory of halteres being specialised hindwings (Bender et al. 1983).

1.2.1 WHAT DO HALTERES SENSE?

Halteres make up only around 0.01% of the body mass in most flies (Pringle 1948). Hence, it is unlikely that they function like balancers, as proposed by Derham. In the early twentieth century, the leading hypothesis was that halteres are organs of stimulation, controlling flight by directly activating flight muscles. This hypothesis was rejected after a comprehensive review of theoretical considerations, anatomical studies, behavioral experiments and electrophysiological recordings, which suggested that halteres are most likely vibrating gyroscopic organs which provided mechanosensory feedback about the flies aerial rotations through Coriolis forces.(Fraenkel 1938, Pringle 1948).

Evolved from hindwings, halteres are driven by the same kinds of muscles that drive wing movements. Three indirect and eight direct muscles modulate the motion of the haltere (Chan et al. 1998). In flight, halteres oscillate in a plane tilted backwards from the transverse plane by around 30°(Nalbach 1994, Dickinson 1999). The angular velocity of the tip of the haltere is almost constant as it moves, with rapid change in direction at the ends (Pringle 1948). In some flies such as *Drosophila* (vinegar flies) (Dickinson 1999), *Calliphora* (blowflies) (Nalbach et al. 1994), and *Hermetia illucens* (soldier flies) (Deora et al. 2015), halteres oscillate anti-phase to the wings. This synchrony of haltere and wing motion is not completely mediated by neural inputs. Pringle suggested that the frequency of haltere oscillations could be locked to wing beat oscillations by mechanical interaction, with the possibility of independence if the natural frequencies of the oscillations are disturbed. A recent anatomical study in *H. illucens*

confirmed that wings and halteres are mechanically coupled by two small ridges of cuticle called sub-epidermal ridges (Deora et al. 2015).

Given the oscillatory motion of halteres in its non-transverse plane, it was theoretically established that rotational forces in all three coordinate axes could be differentiated by halteres (Nalbach, 1993). In Nalbach's simplified description, if the haltere is a point mass, concentrated at the bulb, with a rigid massless stalk, the forces experienced at the haltere are given by:

$$\mathbf{F} = mg - m\mathbf{a}_i - m\mathbf{a}_f - m(\dot{\boldsymbol{\omega}} \times \mathbf{r}_i) - m\boldsymbol{\omega} \times (\boldsymbol{\omega} \times \mathbf{r}_i) - 2m\boldsymbol{\omega} \times \mathbf{v}_i$$

where \mathbf{g} is gravitational acceleration, $(\mathbf{r}_i, \mathbf{v}_i, \mathbf{a}_i)$ encode the position, velocity and acceleration of the haltere end knob relative to the fly, \mathbf{a}_f , the acceleration of the fly; and $\boldsymbol{\omega}$ and $\dot{\boldsymbol{\omega}}$ represent the angular velocity and acceleration of the fly respectively. The different forces in the equation are gravitational (mg), linear acceleration ($m\mathbf{a}_f$), angular acceleration ($m\dot{\boldsymbol{\omega}} \times \mathbf{r}_i$), centrifugal force ($m\boldsymbol{\omega} \times (\boldsymbol{\omega} \times \mathbf{r}_i)$) and the Coriolis force ($2m\boldsymbol{\omega} \times \mathbf{v}_i$).

The strongest of these forces are the primary forces, driving the oscillation of the haltere relative to the fly ($m\mathbf{a}_i$). Among the rotational forces, the Coriolis term ($2m\boldsymbol{\omega} \times \mathbf{v}_i$) dominates over the centrifugal forces. As it is a cross product of the velocity vector, it is dependent on the haltere oscillation frequency. For rotations along pitch, the Coriolis force is lateral to the fly and periodic, with the same frequency as the haltere beating, but at a phase difference of 90° . For rotations along yaw, the forces are lateral to the body, and the frequency is twice that of haltere oscillations. Roll rotations induce radial Coriolis forces.

As the Coriolis forces are distinct for the rotations along the three orthogonal axes, it was hypothesised that halteres sensed Coriolis forces (Pringle 1948). To confirm this, a vibration experiment on tethered *Calliphora* (blowflies) was setup to dissociate the effects of linear acceleration and Coriolis forces (Nalbach et al. 1994). Tethered flies were vibrated such that the effective Coriolis forces for rotations along each rotational axis would be mimiced at the haltere. The compensatory head responses to these imposed vibrations were recorded. Head responses are behaviourally relevant for gaze stabilization in flight. The responses elicited were qualitatively and quantitatively similar to those elicited by real rotations, confirming that Coriolis forces were used for gauging rotational perturbations (Nalbach et al. 1994).

Halteres respond to lateral displacements to its motion (Nalbach et al. 1994). But, roll perturbations manifest as radial forces. The non-orthogonality of the measuring axes, rising from the oscillation of halteres in a plane 30 °from the transverse axis, inputs from both halteres could be used for sensing roll perturbations. (Nalbach, 1994b)

Tethered flight experiments with haltere ablated *Drosophila* show that flies maintain stability against angular rotations by modulating wing stroke frequency and wing stroke amplitude. Pitch rotations increased frequency and amplitude. Roll rotations induced difference in wing stroke amplitude between wings. Unilateral ablation attenuated the response of the ipsilateral wing, but not the contralateral wing (Dickinson 1999).

Behavioural experiments indicate that halteres influence head movements for gaze stabilization and wingstroke kinematics for flight control (Hengstenberg, 1986).

1.2.2 HOW DO HALTERES ENCODE INFORMATION?

Halteres have two kinds of mechanosensory cells at their base; campaniform sensilla and chordotonal organs. In the blowfly *Calliphora* there are 400 campaniform sensilla and 2 chordotonal organs at the base of each haltere (Yarger, 2016).

Chordotonal organs are present under the cuticle. They are sensitive to stretching and vibration of the halteres (Chapman, 2013). Campaniform sensilla are dome shaped protrusions on the surface the cuticle. When the haltere bends, the surface of the dome deflects, activating the mechanosensor and feeding forward to its dendritic projection.

The campaniform sensilla at the haltere base are arranged in five distinct fields; three dorsal fields (dF1, dF2, dF3) and two ventral fields (vF1, vF2). Hence, different directions of deflections of the haltere can be encoded by the haltere. In dF1, dF2, and vF1, the sensilla rows are oriented almost parallel to the axis of the haltere. dF3 and vF2 are oriented perpendicular to this axis.(Chan and Dickinson 1996).

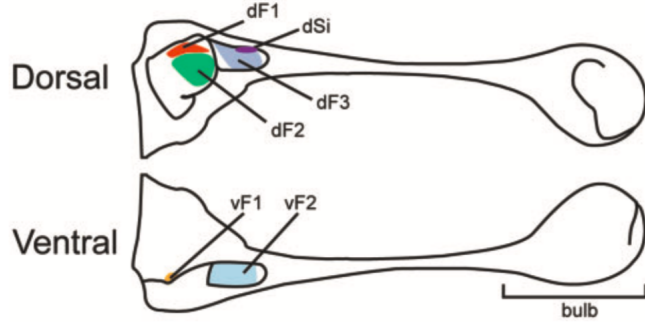


Fig. 3 Diagram showing the haltere campaniform sensilla fields on both the dorsal and ventral sides of the haltere: dorsal Hick's papillae (dF1), basal plate (dF2), dorsal scapal plate (dF3), unbestimmte Papille (dSi), ventral Hick's papillae (vF1), and ventral scapal plate (vF2) (Gnatzy et al. 1987; Chan and Dickinson 1996).

FIGURE 3: Campaniform sensilla fields at the base of halteres. (From Yarger 2016)

The fields dF1, dF3, and vF1 sense vertical primary forces, whereas dF2 and the chordotonal organs are sensitive to lateral gyroscopic forces (Gnatzy et al. 1987). Electrophysiological recordings of the haltere nerve show greater discharge of impulses if the haltere is bent laterally, compared to dorsal or ventral deflections. The haltere nerve rapidly adapts (Pringle, 1948), indicating a potential for quick throughput of sensory information. When the haltere is oscillated, impulses at the haltere nerve are clustered in two volleys per oscillation cycle. Pringle's electrophysiological studies, along with the anatomical descriptions of the campaniform sensilla at the haltere base suggested that rotations along different axes could activate different sensilla populations. The afferent neurons from these populations could have different thresholds for activation. Integrating the neural output of these haltere afferents, could give complete information on rotational instability.

Single-fiber recordings from the haltere nerve in the cranefly, *Holorusia hespera*, with external stimulation of halteres showed that a majority of cells responded linearly to frequencies in the range of wingbeat and twice-wingbeat frequencies. This also supports the theoretical prediction that halteres sense Coriolis forces (Nalbach 1993). Haltere nerve firings are phase locked compound action potentials in response to haltere oscillation (Fox et al. 2008). This hints at another possible mechanism for encoding rotations through halteres; by shifting firing phase of haltere afferents with lateral displacements of the haltere.

Detailed electrophysiological experiments in the flesh fly *Sarcophaga bullata* found evidence supporting both these hypotheses of information encoding; phase shifting and thresholding (Yarger, 2018). A large population of campaniform sensillae having a common coding strategy, and diverse phase sensitivity to haltere motion are capable of quickly detecting numerous forces with fine precision (Fox et al. 2010).

1.2.3 WHAT HAPPENS TO HALTERE INPUTS?

The campaniform sensilla fields at the base of the haltere project to different regions in a fly. Figure 4 shows the haltere afferent projections. In the blowfly *Calliphora* the metathorax is innervated medially by all the dorsal fields, and posteriorly by the ventral fields (Chan et al. 1996). Most projections are ipsilateral, except for the contralateral projections of the dorsal field dF2 and the ventral field vF1.

The complex termination pattern of the campaniform inputs could likely serve to directly route mechanosensory input to appropriate interneurons and motor neurons, for lowering response latencies to rotational perturbations. Extracellular recordings from the wing and neck motor neurons in the blowfly *Calliphora* show ipsilateral and bilateral responses to mechanical stimulation of the haltere, with a very low latency (2 ms), supporting evidence of monosynaptic connections between haltere afferents and motor neurons (Sandeman et al. 1980).

The dorsal campaniform field dF2 directly innervates the synapse at the ipsilateral wing steering motor neuron, mnb1 (motor neuron of the first basalar muscle, b1). The b1 muscle controls wing kinetic parameters by altering the mechanical configuration of the wing hinge. The firing of mnb1 is phase locked with haltere oscillations (Heide 1983). This interaction of dF2 and mnb1 is mediated by a fast monosynaptic electrical pathway (Fayazuddin et al. 1996).

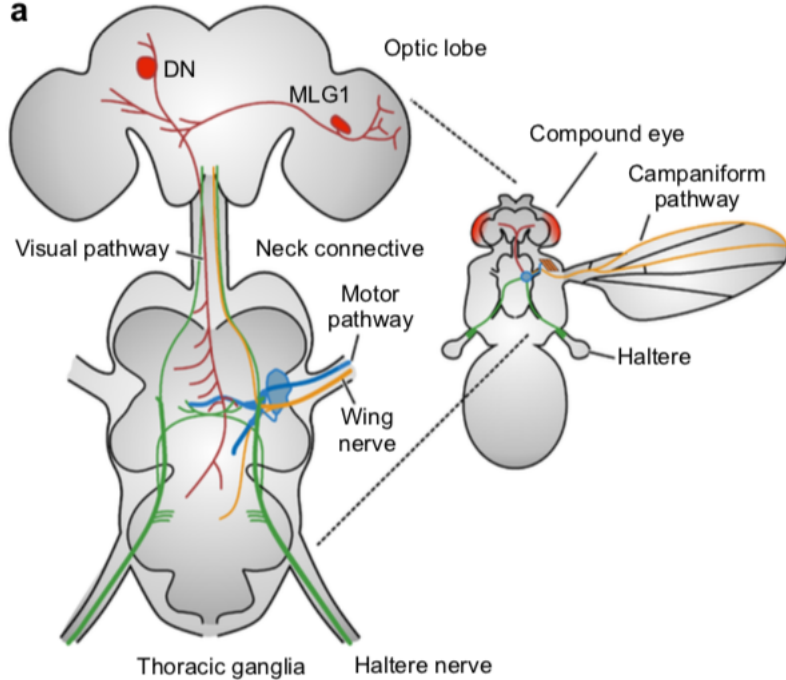


FIGURE 4: Summary of anatomical studies on sensory afferents involved in flight control.
From (Lehmann and Bartussek 2017))

Halteres are not the only source of sensory feedback for mediating control of flight. The fly relies on information from wing mechanosensors for sensing wing deformations (Cole et al. 1982), antennal mechanosensors for airflow sensing (Taylor and Krapp 2008), olfactory inputs, and visual feedback, along with haltere inputs to mediate control of flight (Sherman and Dickinson 2003). Hence, sensory integration across these modalities is relevant for flight control.

There is a strong interaction between visual and haltere inputs towards gaze stabilization and flight control. The haltere system provides rapid feedback on flight perturbations, whereas the slower visual system allows for more accurate feedback (Sherman and Dickinson 2003, Hengstenberg 1991). Some neck motor neurons in the blowfly *Calliphora* respond only when haltere inputs are provided along with visual feedback (Huston and Krapp 2009).

Haltere driving muscles also receive strong excitatory visual inputs. These visual inputs could be actively manipulating the haltere reflex loop for executing voluntary turns without halteres stabilising the induced rotations(Chan et al. 1998). Behavioural studies confirm that haltere inputs are required for executing voluntary turns (Bender et al. 2006).

Control of flight has been mapped in a control theoretical framework to understand how different sensory modalities could be integrated for optimal control of flight. Figure 5 shows some proposed control theoretical frameworks. Deviations from a set point are identified by sensory systems, whose outputs are passed to an integrator, which feeds appropriately to the motor system (Dickinson 2016).

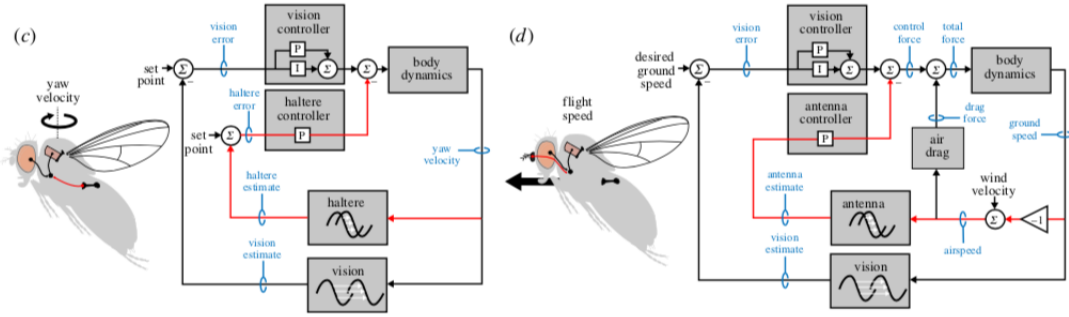


FIGURE 5: Control theoretical models for insect flight, accounting for visual input and mechanosensory inputs. From (Dickinson 2016)

Halteres are also involved in more than just flight control. *Sarcophaga* and *Muscidae* flies oscillate their halteres even as they walk (Hall et al. 2015). In the flesh fly, *Sarcophaga bullata*, haltere ablation impairs ability to walk on vertical surfaces. Haltere ablation in these flies alters their responses to gravity (Daltorio 2018)

1.3 RESEARCH QUESTION AND MOTIVATION

The circuitry of the haltere mechanosensory afferents is known. The mechanisms by which flight can be controlled has been established. Flies can adjust tension in direct wing-steering muscles in response to mechanosensory inputs from the haltere.

Tethered flight studies (Dickinson 1999) show how some wing kinetic parameters change in the absence of halteres. Although tethering flies provides control over experimental conditions, it also changes the physics of the flies, introducing extra forces at the point of tethering. This could potentially have effects on flight dynamics. Hence, conclusions from tethered flight studies cannot be generalised to control in free flight. A proper characterisation of flight is necessary for deciphering possible decoding paradigms of the haltere inputs at relevant muscles.

Unpublished experiments on the effects of haltere inputs in the housefly *Musca* indicate that the wingstroke amplitude of the ipsilateral wing increases on unilateral haltere ablation. To replicate this study in a different model system and to follow up on this study, we set out asking a very simple question:

Do haltere inputs modulate wing beat amplitudes of the ipsilateral wing in free flight

Free flight of unilateral and bilateral haltere ablated soldier flies were filmed using high speed videography to characterise wing kinetic parameters. This study uses a free flight approach to observe flight and its control in its 'natural' form. The outputs of this study will also provide reliable data of wing kinetic parameter modulations in free flight that could be used for better characterisation of the control theoretical frameworks for insect flight control in Dipterans.

Finer analyses of the behavioural effects of haltere input have been limited as flies do not fly well in absence of halteres (Yarger 2016). Nalbach, in her studies used wingstroke frequency as a proxy for wingstroke amplitude (Nalbach 1994a). Dickinson used a photodiode based wing beat analyser for observing stroke amplitude in tethered flight studies (Dickinson 1999). This method provides the relative stroke amplitudes, and not the absolute amplitudes.

Better model systems, higher resolution of high-speed videography, and improved tools for analysing videos make a study on the effects of haltere inputs on wing kinetic parameters in free flight possible.

Hermetia illucens, commonly known as the Black soldier fly, belongs to the family Stratiomyidae, of the order Diptera. Characterised by a black body, this fly ranges from 15 to 20 mm in length (Sheppard et al 2002). The halteres are between 1 - 1.5 mm (Parween et al. 2014). The wing beat frequency in free flight is around 120 Hz. Long visible halteres, along with reasonably stable control in free flight make the soldierfly *H. illucens* an exciting model system for studying flight.

Soldier flies have been used as model systems for studying proprioceptive encoding of head positioning through the prosternal organ (Paulk and Gilbert 2006). The mechanical coupling between halteres and wings was established in soldier flies (Deora et al. 2015). Models for

strain sensing in halteres have also been designed using soldier flies as a template. (Parween et al. 2014)

Soldier flies also have significant commercial potential in waste treatment. The larvae feed on compost and are in turn, efficient, cheap protein sources for poultry and fish cultures. (Sheppard et. al., 2002)



FIGURE 6: A soldier fly; *H. illucens*



FIGURE 7: Closeup of halteres of the soldier fly; *H. illucens*

1.4 REFERENCES

1. Bender, W., Akam, M., Karch, F., Beachy, P. A., Peifer, M., Spierer, P., Lewis, E. B. and Hogness, D. S. (1983). Molecular genetics of the bithorax complex in *Drosophila melanogaster*. *Science* 221, 23-29.
2. Bender JA, Dickinson MH (2006) Visual stimulation of saccades in magnetically tethered *Drosophila*. *J Exp Biol* 209:3170–3182
3. Cole, E. S., and Palka, J. (1982). The pattern of campaniform sensilla on the wing and haltere of *Drosophila melanogaster* and several of its homeotic mutants. *Development*, 71(1), 41-61.
4. Chan, W.P., and Dickinson, M.H. (1996). Position-specific central projections of mechanosensory neurons on the haltere of the blow fly, *Calliphora vicina*. *J. Comp. Neurol.* 369, 405-418.
5. Daltorio K, and Fox. J. (2018). Haltere removal alters responses to gravity in standing flies, *Journal of Experimental Biology* 2018 Jul 25;221 doi: 10.1242/jeb.181719
6. Derham W. (1714). Physico-theology: or, a demonstration of the being and attributes of God, from His works of creation. Being the substance of XVI sermons preached in St. Mary Le Bow-church, London, at the honble Mr. Boyle's lectures, in the years 1711 and 1712 London: W. Innys.
7. Deora T, Singh AK, Sane SP. (2015) Biomechanical basis of wing and haltere coordination in flies. *Proc Natl Acad Sci USA* 112:1481–6.
8. Deora T, Gundiah N, Sane SP. (2017) Mechanics of the Thorax in flies. *Journal of Experimental Biology* 220 (8), 1382-1395
9. Dickinson, M. H., and Tu, M. S. (1997). The function of dipteran flight muscle. *Comparative Biochemistry and Physiology Part A: Physiology*, 116(3), 223-238.
10. Dickinson MH. (1999). Haltere-mediated equilibrium reflexes of the fruit fly, *Drosophila melanogaster*. *Philos Trans R Soc Lond B Biol Sci* 354:903–16.
11. Dickinson, M. H., and Muijres, F. T. (2016). The aerodynamics and control of free flight manoeuvres in *Drosophila*. *Philosophical Transactions of the Royal Society B: Biological Sciences*, 371(1704), 20150388.
12. Fayyazuddin, A., and Dickinson, M. H. (1996). Haltere afferents provide direct, electro-

- tonic input to a steering motor neuron in the blowfly, *Calliphora*. *Journal of Neuroscience*, 16(16), 5225-523
13. Fox, J. L., and Daniel, T. L. (2008). A neural basis for gyroscopic force measurement in the halteres of *Holorusia*. *Journal of Comparative Physiology A*, 194(10), 887-897.
 14. Fox, J. L., Fairhall, A. L., and Daniel, T. L. (2010). Encoding properties of haltere neurons enable motion feature detection in a biological gyroscope. *Proceedings of the National Academy of Sciences*, 107(8), 3840-3845.
 15. Fraenkel, G., and Pringle, J. W. S. (1938). Biological sciences: halteres of flies as gyroscopic organs of equilibrium. *Nature*, 141(3577), 919.
 16. Gnatzky, W., Grünert, U., and Bender, M. (1987). Campaniform sensilla of *Calliphora vicina* (Insecta, Diptera). *Zoomorphology*, 106(5), 312-319.
 17. Hall, J. M., McLoughlin, D. P., Kathman, N. D., Yarger, A. M., Mureli, S., and Fox, J. L. (2015). Kinematic diversity suggests expanded roles for fly halteres. *Biology letters*, 11(11), 20150845.
 18. Hengstenberg, R., Sandeman, D. C., and Hengstenberg, B. (1986). Compensatory head roll in the blowfly *Calliphora* during flight. *Proceedings of the Royal society of London. Series B. Biological sciences*, 227(1249), 455-48
 19. Hengstenberg, R. (1991). Gaze control in the blowfly *Calliphora*: a multisensory, two-stage integration process. In *Seminars in Neuroscience* (Vol. 3, No. 1, pp. 19-29). Academic Press.
 20. Hollick, F. S. J. (1940). The flight of the dipterous fly *Muscina stabulans* Falle in. *Phil. Trans. R. Soc. Lond. B* 230, 383-39
 21. Huston, S. J., and Krapp, H. G. (2009). Nonlinear integration of visual and haltere inputs in fly neck motor neurons. *Journal of Neuroscience*, 29(42), 13097-13105.
 22. Lehmann, F. O., and Bartussek, J. (2017). Neural control and precision of flight muscle activation in *Drosophila*. *Journal of Comparative Physiology A*, 203(1), 1-14.
 23. Nalbach, G. (1993) The halteres of the blowfly *Calliphora*. I. Kinematics and dynamics. *J. Comp. Physiol. A* 173, 293-300.
 24. Nalbach, G. and Hengstenberg, R. (1994a) The halteres of the blowfly *Calliphora*. II. Three-dimensional organization of compensatory reactions to real and simulated rotations. *J. Comp. Physiol. A* 174:695-708.

25. Nalbach, G. (1994). Extremely non-orthogonal axes in a sense organ for rotation: behavioural analysis of the dipteran haltere system. *Neuroscience*, 61(1), 149-163.
26. Parween, R., Pratap, R., Deora, T., and Sane, S. P. (2014). Modeling Strain Sensing by the Gyroscopic Halteres, in the Dipteran Soldier Fly, *Hermetia illucens*. *Mechanics Based Design of Structures and Machines*, 42(3), 371-385.
27. Paulk, A., and Gilbert, C. (2006). Proprioceptive encoding of head position in the black soldier fly, *Hermetia illucens* (L.) (Stratiomyidae). *J. Exp. Biol.*, 209(19), 3913-3924.
28. Pringle, J. W. S. (1948) The gyroscopic mechanism of the halteres of Diptera. *Phil. Trans. R. Soc. Lond. B* 233, 347-384.
29. Sandeman, D. C., and Markl, H. (1980). Head movements in flies (*Calliphora*) produced by deflexion of the halteres. *Journal of Experimental Biology*, 85(1), 43-60.
30. Sheppard, D. C., Tomberlin, J. K., Joyce, J. A., Kiser, B. C., and Sumner, S. M. (2002). Rearing methods for the black soldier fly (Diptera: Stratiomyidae). *Journal of Medical Entomology*, 39(4), 695-698.
31. Sherman, A., and Dickinson, M. H. (2003). A comparison of visual and haltere-mediated equilibrium reflexes in the fruit fly *Drosophila melanogaster*. *Journal of Experimental Biology*, 206(2), 295-30
32. Taylor, G. K., and Krapp, H. G. (2007). Sensory systems and flight stability: what do insects measure and why?. *Advances in insect physiology*, 34, 231-316.
33. Yarger, A. M., and Fox, J. L. (2018). Single mechanosensory neurons encode lateral displacements using precise spike timing and thresholds. *Proc. Royal Soc. B: Biol. Sc.*, 285(1887), 20181759.

CHAPTER 2

METHODS

This study uses soldier flies as a model system to study free flight. To maintain a steady supply of soldier flies, a culture was reared in a greenhouse maintained at 28°C. Physically undamaged flies were collected and the first 20-40 wingbeats in free flight were filmed in a custom setup, at 2800fps using three orthogonally placed synchronised cameras (Phantom V1212, Phantom VEO 640L, Phantom V611). Nikon lenses of 18-70 mm and 24-85 mm were used for the cameras. Filming of free flight was conducted between 0800 hrs and 1300hrs to allow for sufficient natural ambient light. Two bright halogen lamps were used to supplement lighting for high speed filming.

EasyWand5 (Matlab) (Theriault, 2014) was used for calibrating the 3 synchronised cameras. DeepLabCut (Python), a markerless pose estimation tool based on Deep Learning was used to assist in digitising the head, wing tips and wing bases across all frames, along with DLTdv7, (Direct Linear Transform Data Viewer (Ty Hedrick, Matlab)) (Hedrick et al, 2008).

2.1 SOLDIER FLY REARING AND COLLECTION

Soldier flies were reared in a large mesh cage, maintained at 28°C. (Sheppard 2002). A trough with compost was provided for adults to lay eggs in. The compost also served as a source of nutrition for the larvae. The compost was changed twice a week, and the older compost set was moved to a separate container to distill out remaining soldier fly pupae. The larvae would climb the walls of the container and fall out into a second container. The separated pupae were then released into the cage, following which they would crawl into small crevices until they emerged into adult soldier flies.

While collecting flies, flies were examined for damage to wings and antennae. Only flies that maintained sustained flight for more than 5 seconds were collected and used for the study.

2.2 HALTERE ABLATION

The soldier fly was cold anaesthetised by keeping the container with the fly in ice for 3 minutes. Using fine forceps, appropriate halteres were removed from the base. Figure 8 shows a soldier fly with an ablated right haltere.

Post ablation, the flies were stored overnight, in a container with a ball of cotton soaked in water. This is to allow the flies to recuperate from the surgery. Flies were kept in the dark to maintain the natural diurnal cycle and to inhibit flight activity that could cause damage to the wings.



FIGURE 8: Closeup of a fly with an ablated haltere. The wings have been removed for better visualisation of the haltere base. The halteres have been ablated from the base.

2.3 HIGH SPEED FILMING

2.3.1 FRAME RATE

The average wing beat frequency of a soldier fly is around 120 Hz, i.e. the wing beat period is around 8.3 milliseconds. To properly characterise wingbeat parameters, a significant number of frames in each wing-beat period is required. Figure 9 explains why this is required, using a periodic function, $\sin(x)$. Setting the number of frames required per wing beat at 20, the

frame rate to capture flight of a soldier fly should be greater than 2400 fps.

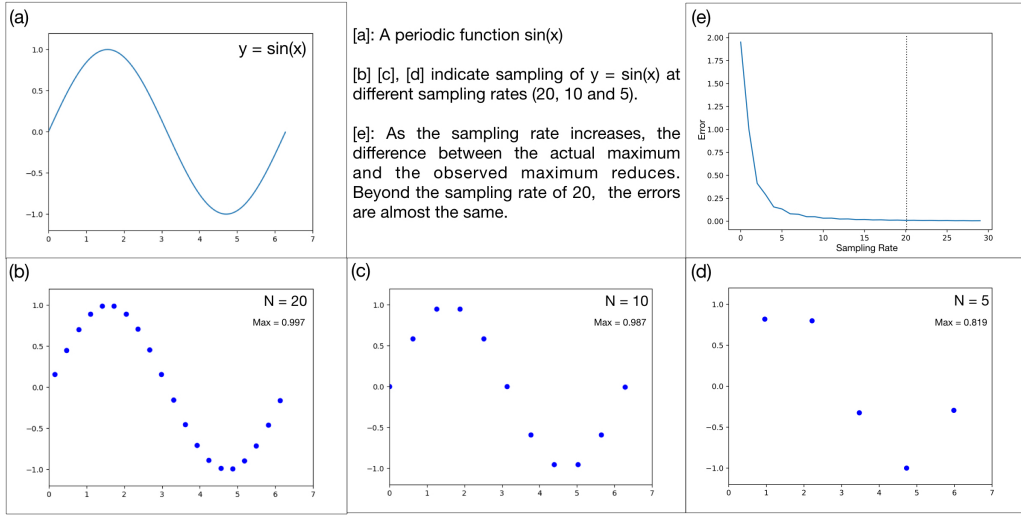


FIGURE 9: Sampling Rate of 20 for a smooth periodic function gives a reasonable estimate of the function.

2.3.2 RESOLUTION

An image is simply a representation of an 3D environment on a finite 2D region. For a given distance from the camera, the least count for the measurement of length of an object is defined by the number of pixels on the sensor. Higher the resolution of the video, lower the 'least count' and therefore, lesser the errors in representation of objects.

The memory of the camera is finite. Hence, as resolution is increased, the maximum possible frame rate reduces. To maximize the frame rate while maintaining a decent resolution, the frame rate was set at 2800 fps.

2.3.3 EXPOSURE TIME

The wing length of a soldier fly is on the order of 1 cm. The wing beat frequency is around 120 Hz. Considering that the wing moves around 120 °from tip to tip, the radial velocity of the wing tip is around 5 m/s. ($v = 4\pi r f / 3$, where r is length of the wing and f is frequency. $4\pi/3$ corresponds to 240 °, which is approximately the angle covered in one wing beat)

If the exposure time is too high, the representation of the wing tip on the image will move

across multiple pixels, causing pixel blurring. In $100 \mu\text{s}$, the wing tip moves around 0.5 mm, a negligible change at the camera sensor for the lens used and the distance of the fly from the lens. Hence, the exposure time was chosen to be $100 \mu\text{s}$.

At this low level of exposure, an image will be extremely dark unless strong sources of external lighting is present. To account for this, 2 strong halogen lamps were used to illuminate the filming region.

2.3.4 MULTICAMERA SETUP

Videos taken from a single camera are not sufficient for extracting 3D coordinates. To reconstruct in 3 dimensions, at least 2 camera views are required. Also if multiple cameras are used, the videos recorded from all the cameras need to be synchronised, i.e. the shutters need to open and close in synchrony.

Each camera has an internal clock. When multiple cameras are externally F-synced, the clock inputs from a master camera drives the other (slave) cameras, overriding the internal clocks in the slave cameras. The Phantom high speed cameras have a 56 MHz clock, corresponding to a timing least count of 17.875 ns. Therefore, the frames captured by the multiple synced cameras are within 20ns, which is extremely small compared to the timescale of the frame rate($350 \mu\text{s}$). (*Phantom Camera Manual*)

The sync and trigger timing was confirmed by filming an LED panel as it switched on. If the LED panel lit up in the same frame in all videos, the cameras were synchronised. Else, the camera connections were re-done and the test was repeated.

Phantom cameras have a fixed internal memory capacity. When the cameras are active, film is continuously written into this internal memory, over-writing the earlier memory in a cycle, ensuring that only the previous n seconds remain in memory (n being a constant, depending on the memory and resolution of images). Once an external input, a trigger, is activated, the over-writing stops and the entire memory can be transferred to a the computer and saved.

For multiple cameras, the same external trigger input can be used for all cameras by appropriate wiring in the setup.

When filming from multiple views, a transformation method is required for converting pixel coordinates from all the cameras to coordinates in real space. The Direct Linear Transform method has been used in this study (Hartley, 2003).

Direct Linear Transform

Every point in the real space (x,y,z) is represented as a (u,v) on an image from a camera. This representation depends on the position of the point relative to the camera, and the physical parameters of the sensor on the camera.

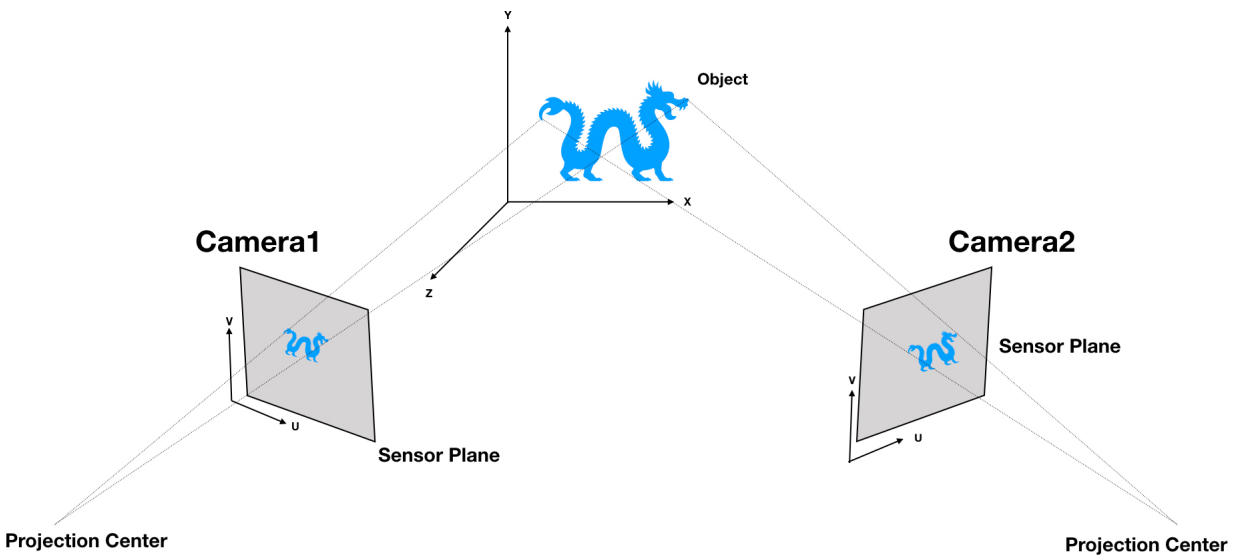


FIGURE 10: Representation of 3D space on camera sensors

For a given camera, if there are multiple known (x,y,z) and corresponding (u,v) points, the reprojection centre can be identified. With this reprojection centre, given an (u,v) point, a line of possible points in the real space can be calculated.

With known (x,y,z) and corresponding (u_i, v_i) points from multiple cameras, a proper reconstruction matrix can be identified. Each camera point (u_i, v_i) would give a line as a solution. The point in real space is given by the intersection of these lines. The Direct Linear Transform method uses the method of least squares to find the solution of these lines. Simply put, a point is identified such that the sum of distances from the point to each line is minimized. Therefore, even if the lines do not intersect, a solution can be estimated.

The reconstruction method requires identification of a set of coefficients, estimated using the known (x,y,z) and (u_i , v_i) points. This process of estimating the variables is called calibration. The Direct Linear Transform uses 11 coefficients to code for the intrinsic properties of a camera placement. For the purpose of our discussion, let them be L_i . The transformation matrix to obtain (x,y,z) coordinates from camera pixel coordinates using this method is: (Hartley, 2003):

$$\begin{bmatrix} u^{C1} - L_4^{C1} \\ v^{C1} - L_8^{C1} \\ u^{C2} - L_4^{C2} \\ v^{C2} - L_8^{C2} \end{bmatrix} = \begin{bmatrix} (L_1^{C1} - u^{C1}L_9^{C1}) & (L_2^{C1} - u^{C1}L_{10}^{C1}) & (L_3^{C1} - u^{C1}L_{11}^{C1}) \\ (L_5^{C1} - v^{C1}L_9^{C1}) & (L_6^{C1} - v^{C1}L_{10}^{C1}) & (L_7^{C1} - v^{C1}L_{11}^{C1}) \\ (L_1^{C2} - u^{C2}L_9^{C2}) & (L_2^{C2} - u^{C2}L_{10}^{C2}) & (L_3^{C2} - u^{C2}L_{11}^{C2}) \\ (L_5^{C2} - v^{C2}L_9^{C2}) & (L_6^{C2} - v^{C2}L_{10}^{C2}) & (L_7^{C2} - v^{C2}L_{11}^{C2}) \end{bmatrix} \begin{bmatrix} x \\ y \\ z \end{bmatrix}$$

FIGURE 11: DLT 3D reconstruction matrix

where u^{C^i} and v^{C^i} represent the pixel coordinates of the camera C_i , $L_j^{C_i}$ represents the j^{th} DLT coefficient of camera C_i . The equation can be represented by the matrix equation, $Y = AX$. The matrix X, which codes for the 3D coordinates can now be calculated using the least squares method.

If the camera is moved, or if focus or zoom are changed, the transformation matrix changes. Hence, for every camera configuration, calibration is required. As our videos required accuracy at the order of 1 pixel over a large region, the tool, EasyWand5, from Ty Hedrick (Theriault, 2014) was used. To use this method, a thin quartz capillary (1 mm outer diameter) of length 7.5cm, with marked ends was waved around the filming. These points were then manually marked and passed to the EasyWand5 tool, along with the parameters of the sensors on the camera. The tool then estimates the DLT coefficients, reprojection errors, and a wand score, a representation of how the quality of the calibration. If the reprojection errors were less than 1 pixel for all cameras, the calibration was considered good. Calibration videos were taken twice for each day of filming, once after setting up the cameras and once after collecting flight bouts.

TABLE 1: Parameters of Cameras and Lenses used. (From Phantom Camera Data Sheet)

Camera ID	Lens Focal Length	Sensor Pixel Size	Resolution
V1212	85 mm	28 μ m	1200 x 800
V611	70 mm	20 μ m	1200 x 800
VEO 640L	85 mm	10 μ m	1920x1080

EasyWand5 uses the focal lengths of lenses and the physical parameters of the image sensor to generate preliminary estimates of the DLT coefficients. These parameters are outlined in the above table. Using the 8 point algorithm (Hartley, 2003), labeled wand points, and a refinement method, Sparse Bundle Adjustment, the DLT coefficients are calculated. Although the underlying principle of this method does not require a wand, the end points aid in checking calibration errors, as the distance between these points is a known constant, 7.5 cm.

2.4 FLIGHT INITIATION PARADIGM

For optimal filming of flight, a method for consistent initiation of flight is required. The following constraints needed to be addressed:

1. The region in view while filming should be small. Smaller the region, the more the number of pixels representing the fly in flight
2. The fly should have enough space to fly without hitting a surface
3. There should be an easy mechanism to allow capture of flies after filming flight

With these constraints in mind, a setup as shown in Figure 12 was designed.

The box is a 100cm x 100cm x 80cm (lxbxh) chamber. All but two faces are made of acrylic. The side face is fitted with a piece of thermocol, with a hole large enough for a falcon. This side can be removed during the experiment without disturbing the rest of the setup. The box is kept on a table, along with two halogen lamps for sufficient illumination. Three cameras are set up as shown in the figure, to obtain almost orthogonal views of the filming region.

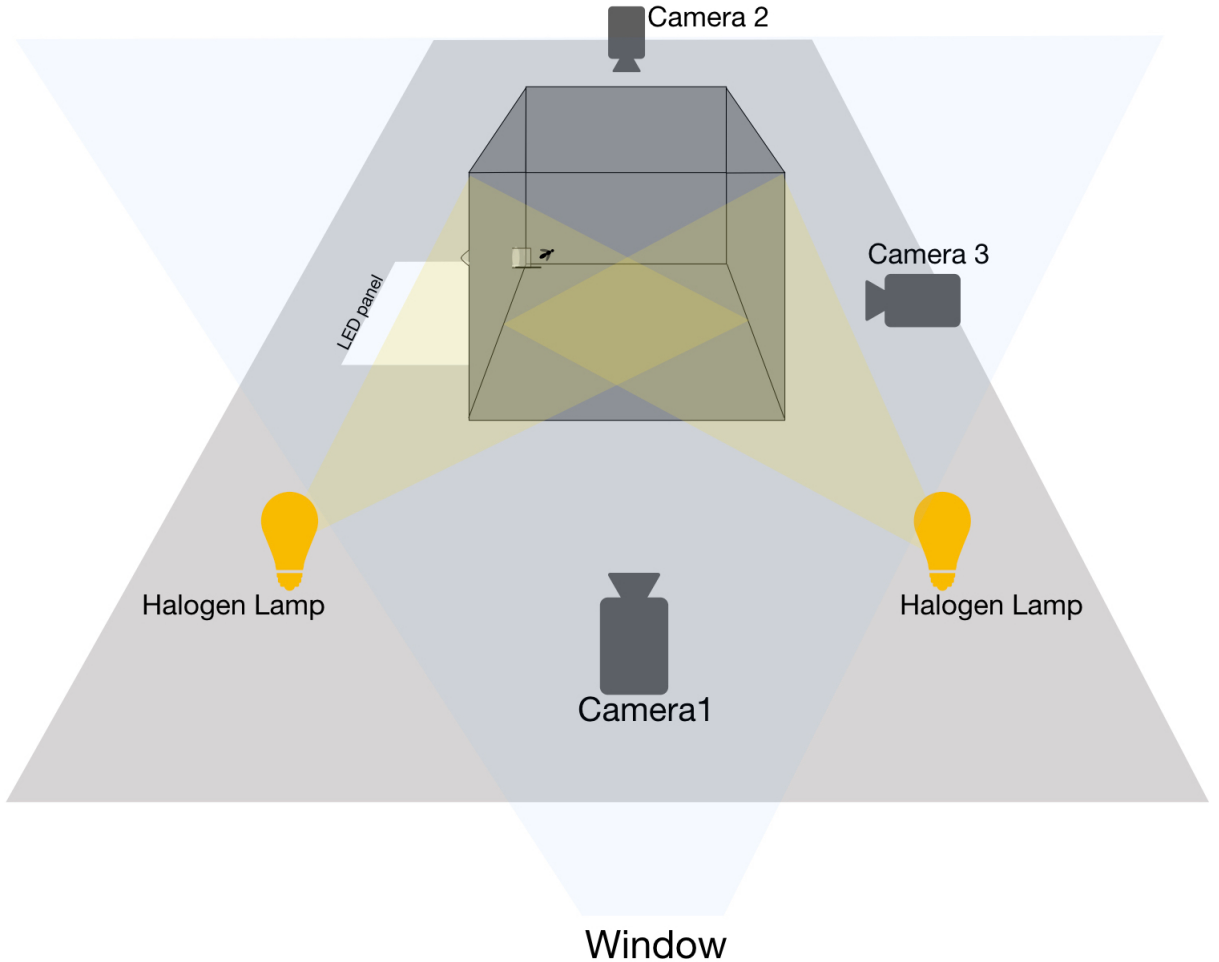


FIGURE 12: Setup for High Speed Filming of Free flight of soldier flies

Flies were kept in a falcon, along with an ice-cream stick. When the falcon was opened inside the chamber, the fly would either walk to the end of the stick, or climb to the outside of the falcon and initiate flight. If the fly inside the falcon didn't move, the falcon was rotated gently to incite the fly to move to the end of the falcon and initiate flight. In the absence of the ice cream stick, the fly would start flying from the edge of the falcon, resulting in the first few wingbeats being hindered by the falcon tube.

After filming flight, the fly would be recaptured in a falcon. Soldier flies are much easier to handle, compared to houseflies and can be captured without damage to the fly.

The falcon was covered with tissue paper. The tissue acts like a diffuser for the light source kept under the falcon, so as to prevent a dark spot in the video. (For Camera 3 in Figure 12)

2.5 DIGITIZATION

Once the flight bout has been filmed, appropriate points on the fly need to be marked on each frame of the video for further analysis. This process of extracting the array of relevant pixel coordinates from the video is digitization.

A plethora of tracking tools (Hedrick et al, 2008) are available, that aid in digitization. But, these require an external marker to be added at the relevant points. Adding multiple external markers on the flies could hinder with their flight capabilities, and alter the behaviour of interest to this study. Without external markers, manual digitization is a very slow process. For this study alone, digitisation would have required more than 500,000 mouse clicks for manually identifying relevant points on images. The MATLAB based DLTdv7 tool is among the more popular softwares that provide an user interface for digitization (Hedrick et al., 2008).

With the advent of Machine Learning and its extension to image processing, softwares adapting these power horses for digitising behavioural tracking videos are being introduced. Over the past year, two tools, Leap (Pereira et al., 2018) and DeepLabCut (Mathis et al., 2018) have been published. This study has relied on DeepLabCut for aiding in digitisation.

2.5.1 DEEPLABCUT

DeepLabCut is a deep learning tool that is based on DeeperCut (Insafutdinov et al., 2016), a pose estimation paradigm. To properly understand how DeepLabCut works, it is important to understand the following:

1. **Feature Detection in Images** Images are arrays of pixel intensities. Local distributions of intensities in an image can correspond to features in the image, such as edges, ridges, corners and blobs. As a computer algorithm cannot make coherent sense of an image as a whole, it breaks down the image into a summation of features, which can then be processed to estimate what the image represents.

In the case of soldier fly images, the closest feature representing a wing tip is a corner with edges at specific angles. The point representing the head could be an intersection of a blob and two edges (antennae).

2. **Neural networks** Consider a system that takes in multiple inputs, and gives a single output. It performs some operations on the inputs, with different 'weights' for each input and calculates a function of these inputs to spout out a single binary output. This unit, a perceptron is the simplest representation of a neural network (Neilsen, 2015). (Rest of this section refers to the same book)

If multiple perceptrons exist in a networked fashion, each receiving multiple inputs, performing weighted calculations on these inputs and then passing on the outputs to other layers of perceptrons, a complete neural network is obtained. The outputs depend on the weights of each input to a perceptron and the architecture of the network, i.e. the number of perceptrons in each layer.

In our system, the input layer would be the inputs from all the pixels, and the output layer would be the points on the fly we are interested in.

To make a neural network 'learn' involves tweaking the weights for each perceptron to match a set of provided inputs to its provided output, with the hope that the trained network can generalise to beyond the provided inputs and can be used on any appropriate input.

One of the efficient, well performing methods to find the set of weights that minimise the cost function is Gradient Descent. With an initial estimate, the weights are tweaked and the performance of the tweaked network is calculated using a cost function, comparing the output of the network to the expected output. The next iteration of this process uses the tweaked weights that reduced the cost function the most, nudging the set of weights towards a minima. As this process is repeated over and over, a set of weights that minimize the cost function pretty well are found. This method may not provide the best solution, but it provides a reasonably well performing solution.

The depth of a neural network is the number of different layers present in it. The deeper the network, the more robust it can be once properly trained.

To reduce computational complexity in deep neural networks, convolutional architecture of the neural network is used. These are very useful for image analysis. In Convolutional neural networks, the perceptrons in a layer take inputs only from a subset of the perceptrons in the previous layer, with 'neighbouring' perceptrons having a large set of shared

inputs. The outputs at this 'convolutional layer' are pooled together to create 'pooling layers', forming condensed feature maps from the outputs local receptive fields, which can be fed forward in the neural network.

If the architecture allows inputs from a layer to synapse to perceptrons in layers not immediately following it, in convolutional networks, the network is termed as a residual network. These types of networks allow for a system to understand more global features of the input layer.

ResNet50 is a residual neural network with 50 layers. ResNet101 and Resnet152 are also variants of residual networks that can be used for image classification. In this study, the resnet50 architecture has been used.

3. DeepLabCut

DeepLabCut is a deep learning based software tool that can be used for markerless pose estimation for quantifying behaviour. It utilises a state of the art (as of 2018) feature detectors that were designed for DeeperCut, a multi person pose estimation tool (Insafutdinov, 2016).

It uses a residual network, resnet50, pre-trained on ImageNet, as the initial network architecture for training. Using a pre-trained network reduces the computational complexity of implementing deep learning for a specific target. This form of 'transfer learning' allows for robust and data efficient rewiring of the network.

DeepLabCut allows an user to provide multiple training images and the coordinates of relevant points, which are then used to create a trained network that can generalise to labeling complete videos.

DeepLabCut is advantageous as it allows for post hoc analysis of behavioural videos, and no external marker that can potentially hinder with the behaviour being studied is required.

2.5.2 DEEPLABCUT FOR POSE ESTIMATION

DeepLabCut runs on Python3. It has the following modules:

a) Create New Project

Creates a new folder with the basic files required for using the software

b) Label Images

A Graphical User Interface (GUI) that allows the user to choose images to label and label them with appropriate points

c) Create Training Dataset

Reformats labeled images and points into a single folder that the training algorithm reads from

d) Train Network

Uses transfer learning on a pre-trained residual neural network, using the labeled images

e) Evaluate Network

Checks the quality of the trained network on a subset of labeled images and confirms its performance.

f) Analyze and Label Videos

Labels videos using the trained network and outputs files with the labeled points.

g) Refine Training Dataset

If some labels in Step7 were off, then they can be relabeled and the network can be retrained.

We use modules (a), (c), (d), (e) and (f) from DeepLabCut for the purpose of this study.

Labelling for Training the Network

As DeepLabCut's labelling GUI only shows extracted images and displays them individually for labelling, I wasn't able to consistently and accurately mark points across all frames. To overcome this challenge, I labeled random frames on DLTdv7, which allowed for comparing the frame of interest with preceding frames in the video, and also gave DLT residual errors for marked points across cameras. These factors allowed for easier, more consistent labelling,

that could be used for sensible 3D reconstruction. The interfacing of DLTdv7 and DeepLabCut was achieved by a custom-made Python based script, along with scripts from the first release of DeepLabCut (DLC 1.0). Another advantage of using this method over DeepLabCut's GUI is that the images used for training are cropped tightly, reducing the memory and time requirements for training the network.

A total of 520 images from 25 videos were labeled and prepared for training to ensure diversity of the training set. Separate networks were trained for each camera view.

GPU requirements for Training

DeepLabCut uses Tensorflow based neural network training. It iteratively modifies the weights in a residual neural network, pre-trained on ImageNet, a massive dataset for object recognition, with over 14 million hand annotated images. DeepLabCut uses 1,030,000 iterations by default to change the weights of the pre-trained network.

Transfer learning on a pre-trained network is still a computationally heavy task and requires significant GPU allocation. Multiple methods were used to facilitate training.

1. GPU cluster @ NCBS: Pakeeza

To get DeepLabCut working on the GPU cluster, some tweaks and modifications were required. The details of these can be found on the project Github page.

2. Google Colab

Google Colab is a service that provides a platform for the everyday person to learn and implement machine learning, without having to invest in expensive computational hardware. Colab provides access to a GPU, with 12GB memory, for 12 hours at a time. (Tesla K40 systems). DeepLabCut was packaged with scripts that could be run on the Google Colab platform.

3. In House Laboratory Computer

The inhouse laboratory computer has a GTX 1080 8GB GPU unit, which is extremely powerful and more than sufficient for training networks.

Labeling Videos on DeepLabCut

Once the network is trained using the labeled images, it can be used for unlabeled videos. Figure 13 shows the accuracy of the trained network.

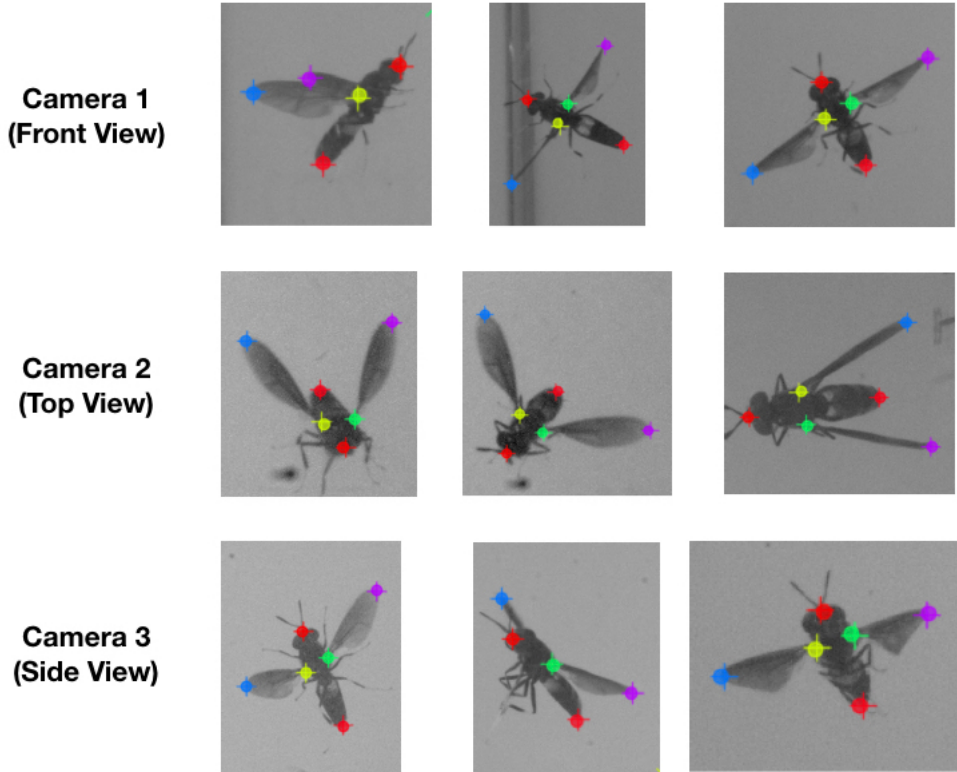


FIGURE 13: Outputs of DeepLabCut labeling. For all three views, separate networks were trained. The outputs here compare manually labeled points (circle points) and the estimates of the trained network (+ points)

Confirming Labels

The labels estimated by DeepLabCut are not 100% perfect. For robust analysis, it was important to have accurate and precise annotations. The labeled outputs from DeepLabCut were reformatted into files that could be read by DLTDV7 and the labels were confirmed manually.

3D coordinates were reconstructed from the points digitised by DeepLabCut using the DLT calibration matrix, obtained using EasyWand5. The 3D reconstruction fit is a solution of a linear system of equations using a least squares method. The sum of distances between real

and reprojected points from the solution; the residual, is used as an estimate of the ‘goodness’ of the 3D reconstruction fit.

While reformatting, if the DLT residuals for the labeled points were more than a certain threshold, only the pair of views having the least DLT residual was considered. Else, all the labeled points were used for reformatting.

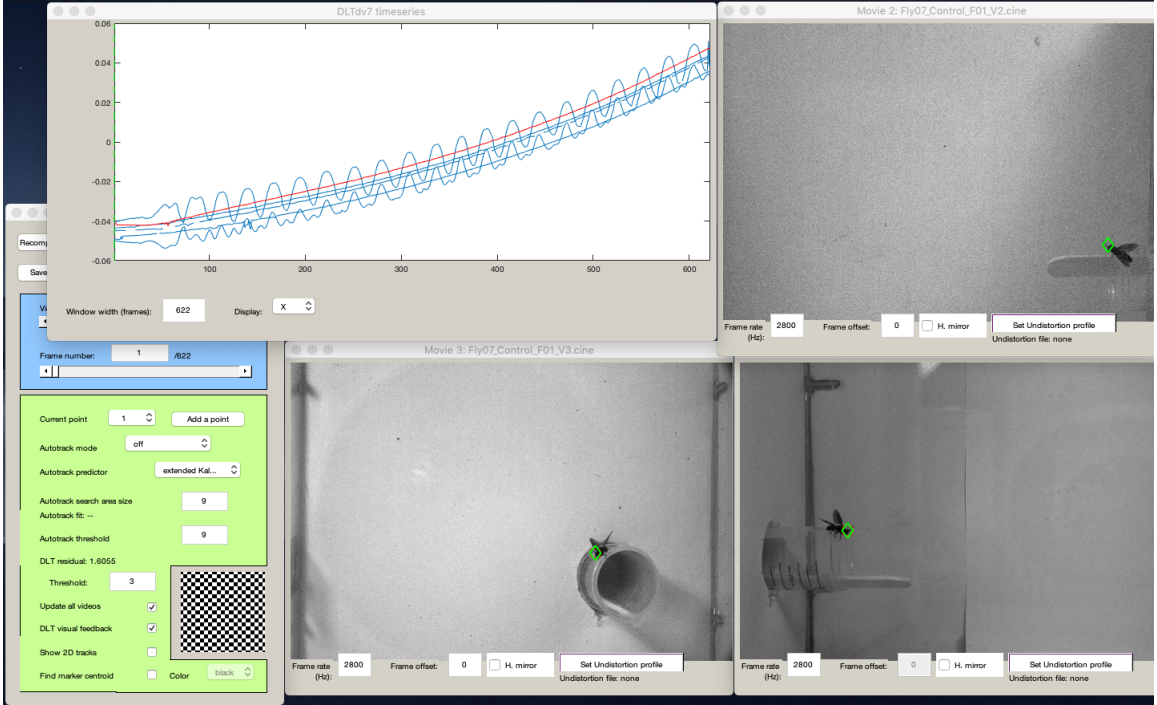


FIGURE 14: Outputs of DeepLabCut labelling, converted to DLTdv7, on the DLTdv7 GUI. Note the DLTdv7 time series indicates mostly smooth plot trajectories, indicating the performance of reconstruction from the points labeled by the trained network.

Improving DeepLabCut

At its core, DeepLabCut basically assigns weights to a network to minimize a ‘cost function’. In its current form, DeepLabCut only tries to reduce the residual between labeled points and estimated points in each frame. For better performance in contexts relevant to studying behaviour, the following could be factored into the cost function when training the network:

- 1. Tracking Across Frames** Currently, DeepLabCut analyses videos frame by frame; each frame individually. In a high speed video, relevant points would not be expected to move drastically across consecutive frames. The distance between the current point estimate

and the estimate in the previous frame could be used as a numerical estimate for this feature.

2. **3D reconstruction DLT residual minimization** When using multiple cameras, the DLT residual is a good estimate of whether the points digitised across videos correspond to the same point in real 3D space.

Implementing the above would affect the computational complexity involved in training the network, but with the current availability of computational power, incorporating the above is certainly within reach.

Also, DeepLabCut is still in development and a lot is required in terms of user interfacing. To circumvent the disadvantages posed by DeepLabCut's GUI, a custom code was used for this study, as explained in the earlier sections.

The following flowchart summarizes the digitization protocol:

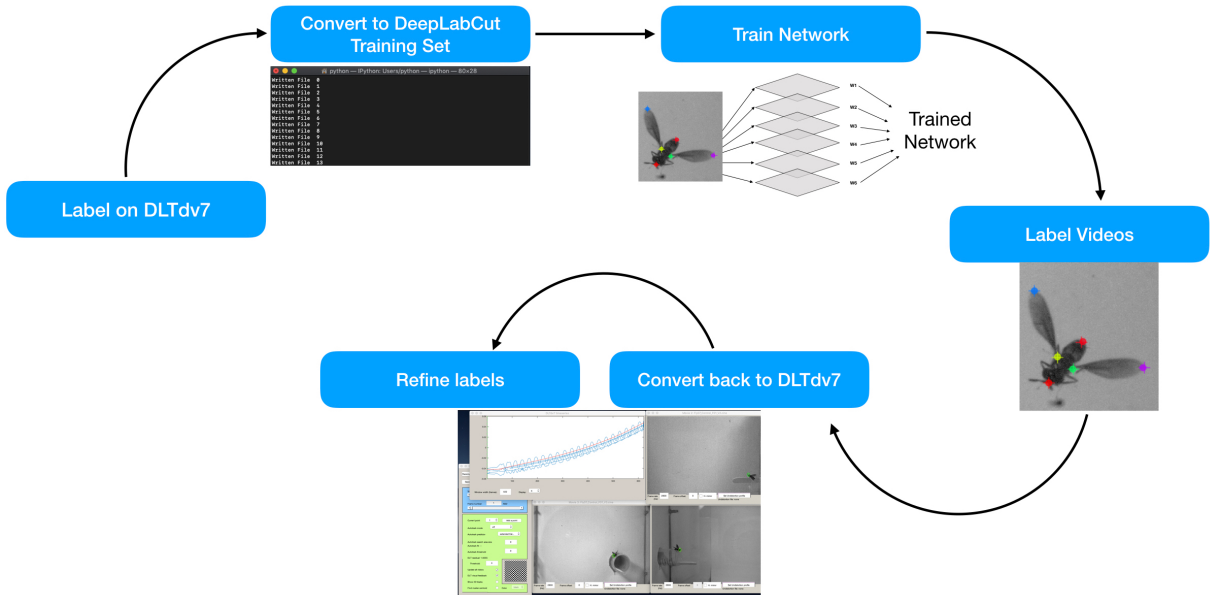


FIGURE 15: Flowchart outlining protocol used for Digitization

All codes written for digitization can be found at

https://github.com/aiyeraditya/SoldierFly_FreeFlight

2.6 REFERENCES

1. Michael A. Nielsen, "Neural Networks and Deep Learning", Determination Press, 2015
2. Insafutdinov, E., Pishchulin, L., Andres, B., Andriluka, M. and Schiele, B. DeeperCut: a deeper, stronger, and faster multi-person pose estimation model. in European Conference on Computer Vision 34–50 (Springer, New York, 2016).
3. D. Craig Sheppard, Jeffery K. Tomberlin, John A. Joyce, Barbara C. Kiser, Sonya M. Sumner, Rearing Methods for the Black Soldier Fly (Diptera: Stratiomyidae), Journal of Medical Entomology, Volume 39, Issue 4, 1 July 2002, Pages 695–698, <https://doi.org/10.1603/0022-2585-39.4.695>
4. Richard Hartley and Andrew Zisserman (2003). Multiple View Geometry in computer vision. Cambridge University Press. ISBN 978-0-521-54051-3
5. Theriault, Diane H. et al "A protocol and calibration method for accurate multi-camera field videography." Journal of Experimental Biology (2014): jeb.100529.
6. Hedrick, T. L., Software techniques for two- and three-dimensional kinematic measurements of biological and biomimetic systems, Bioinspiration and Biomimetics, 2008
7. Mathis, Alexander, Pranav Mamidanna, Kevin M. Cury, Taiga Abe, Venkatesh N. Murthy, Mackenzie Weygandt Mathis and Matthias Bethge. "DeepLabCut: markerless pose estimation of user-defined body parts with deep learning." Nature Neuroscience 21 (2018): 1281-1289.
8. Pereira, Talmo D, Diego E. Aldarondo, Lindsay Willmore, Mikhail Kislin, Samuel S-H Wang, Mala Murthy and Joshua W. Shaevitz. "Fast animal pose estimation using deep neural networks." Nature Methods 16 (2018): 117-125.

CHAPTER 3

ANALYSIS AND RESULTS

3.1 ANALYSIS

For this project, three flight bouts were filmed per fly before and after treatment (*cold anaesthesia and haltere ablation*). A total of 15 flies in 4 treatment groups; right haltere ablated, left haltere ablated, both halteres ablated and a control group. Due to time constraints, only one flight bout after treatment was analysed for 7 flies in three treatment groups; right ablated, left ablated and control. Although the flight of bilateral haltere ablated flies would help in testing our hypothesis, it is not necessary.

After 3D coordinates were digitised for each flight bout, the following parameters were calculated.

1. Body Angles: Pitch, Roll and Yaw

The vector joining the left wing base to the right wing base was constructed. The elevation of this vector from the XY plane is considered to be the roll angle. If a fly is flying parallel to the ground, this vector is parallel to the XY plane; zero elevation. As the fly rolls, this vector has a non zero projection on the Z Axis, and therefore, a non zero elevation.

For calculating pitch, a vector joining the head to the mid point of the wing bases was constructed. The elevation of this vector with respect to the XY plane is considered to be the pitch angle. As the fly pitches up, the elevation of this vector increases.

Consider the projection of the roll vector (joining the two wing bases) on the XY plane. The angle made by this projection with the X Axis is considered as the yaw angle.

Figure 16 shows how these constructed vectors change as the fly moves.

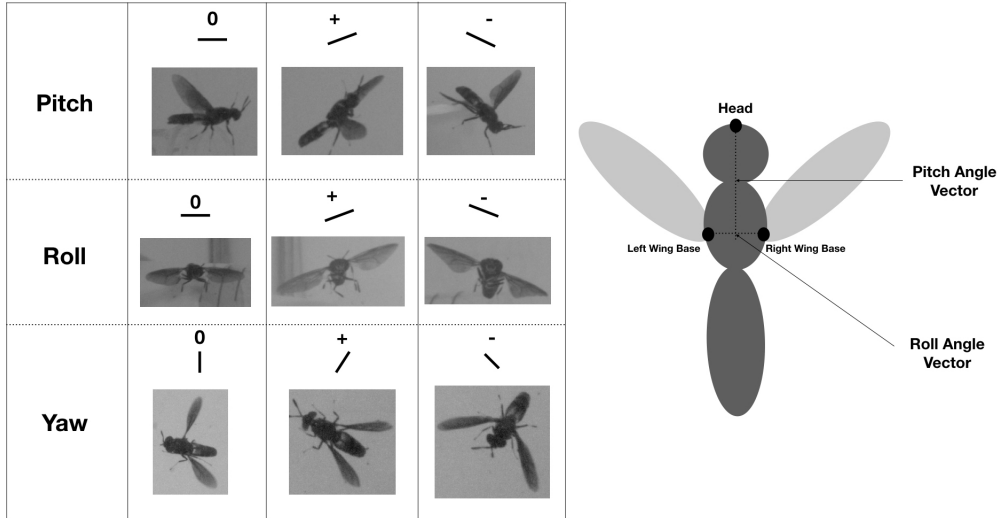


FIGURE 16: The elevation of the vector joining the wing bases changes with roll. The elevation of the vector joining the head to the mid point of wing bases changes with pitch. These two vectors are perpendicular to each other. The azimuthal of these vectors changes with yaw.

2. Wing Kinematic Parameters: Stroke Angle and Deviation Angle

Wing kinematic parameters were calculated using a custom MATLAB code, written by Ty Hedricks and modified by Dinesh Natesan.

For our digitised data, the time evolution of the stroke angle did not require filtering for analysis of peaks. On the other hand, the deviation angles gave lots of false positive peaks when analysed without filtering. Hence, the deviation angles were filtered using a third order Butterworth filter, with sampling frequency at 2800 Hz and cutoff frequency at 400 Hz. These parameters gave the least difference between the real data and the filtered data (Figure 17).

The peaks and troughs for these wing kinematic parameters were calculated using the built-in MATLAB function: 'findpeaks'. For each fly, the means of the positive and negative peaks were calculated. The positive peaks were defined as ventral excursion maxima and the negative peaks as the dorsal excursion maxima. The difference between the means was defined as the peak to peak amplitude. Subtracting the means is equivalent to calculating individual peak to peak amplitudes and then averaging them (Figure 18)

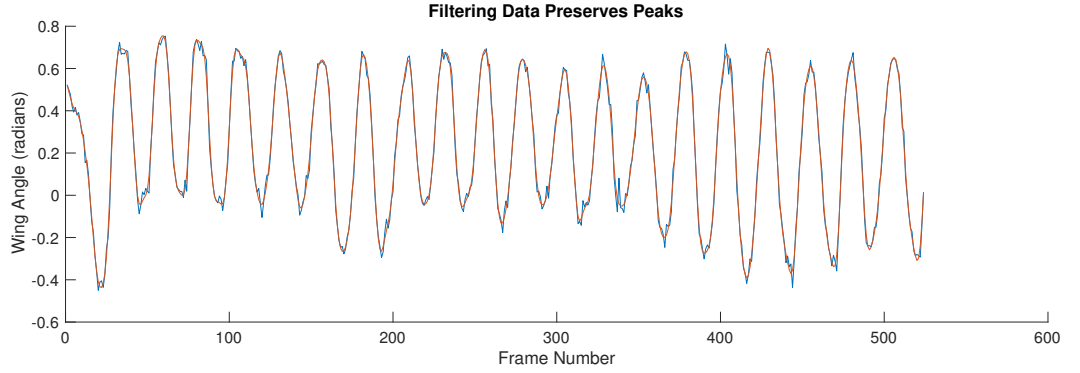


FIGURE 17: Raw data (blue) and filtered data (orange) for deviation angle. The peaks are mostly preserved through filtering. The filter used is a third order Butterworth filter with sampling at 2800 Hz and cutoff at 400 Hz

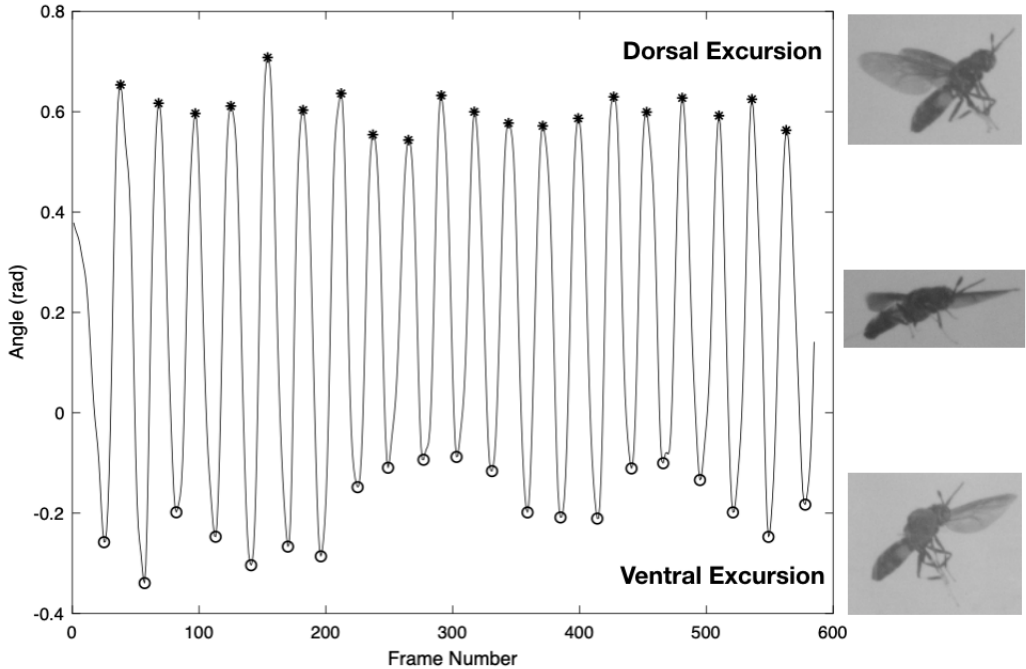


FIGURE 18: A plot showing the time evolution of deviation angle. Peaks have been labeled. The positive peaks correspond to dorsal excursion maxima. The negative peaks correspond to ventral excursion maxima. The images of the fly approximately show the pose of the fly for the corresponding angles on the Y axis.

For the first 20 wing strokes in all flies, dorsal excursion, ventral excursion and peak to peak amplitudes for stroke angles and deviation angles were compared across the treatment groups. 20 wing strokes was chosen to maintain consistency, given the constraint of the small filming volume. This corresponds to around 200 ms, which is a long enough time to observe perturbations and the fly's response. In comparison, the time scale of visual feedback controlling flight

is 25-30 ms, as discussed in Chapter 1.

As there are only 7 data points per treatment group and three groups, a Kruskal Wallis test was used for statistical analysis. The Kruskal Wallis test is a non parametric method of testing if samples originate from the same distribution. It can be used for independent samples. Being non parametric, it does not assume a normal distribution of the residuals. Given that the data across treatment groups are expected to be independent, the Kruskal Wallis test is suited for statistical analysis of our collected data. The null hypothesis for a Kruskal Wallis (KW) test is that the medians of the samples in each group are equal. When this null hypothesis is rejected, pairwise comparisons were done using the Wilcoxon rank sum test to identify the pairs of the treatment groups which differ.

All software used for analysis, with the exception of Dinesh Natesan's code for obtaining wingstroke angles, were written by me. These can be found at

https://github.com/aiyeraditya/SoldierFly_FreeFlight, along with wing kinematic plots for each analysed fly.

3.2 RESULTS

3.2.1 BODY ANGLES

Time Evolution of Body Angles

The time evolution of the body angles was plotted for all analysed flies (Figure 19)

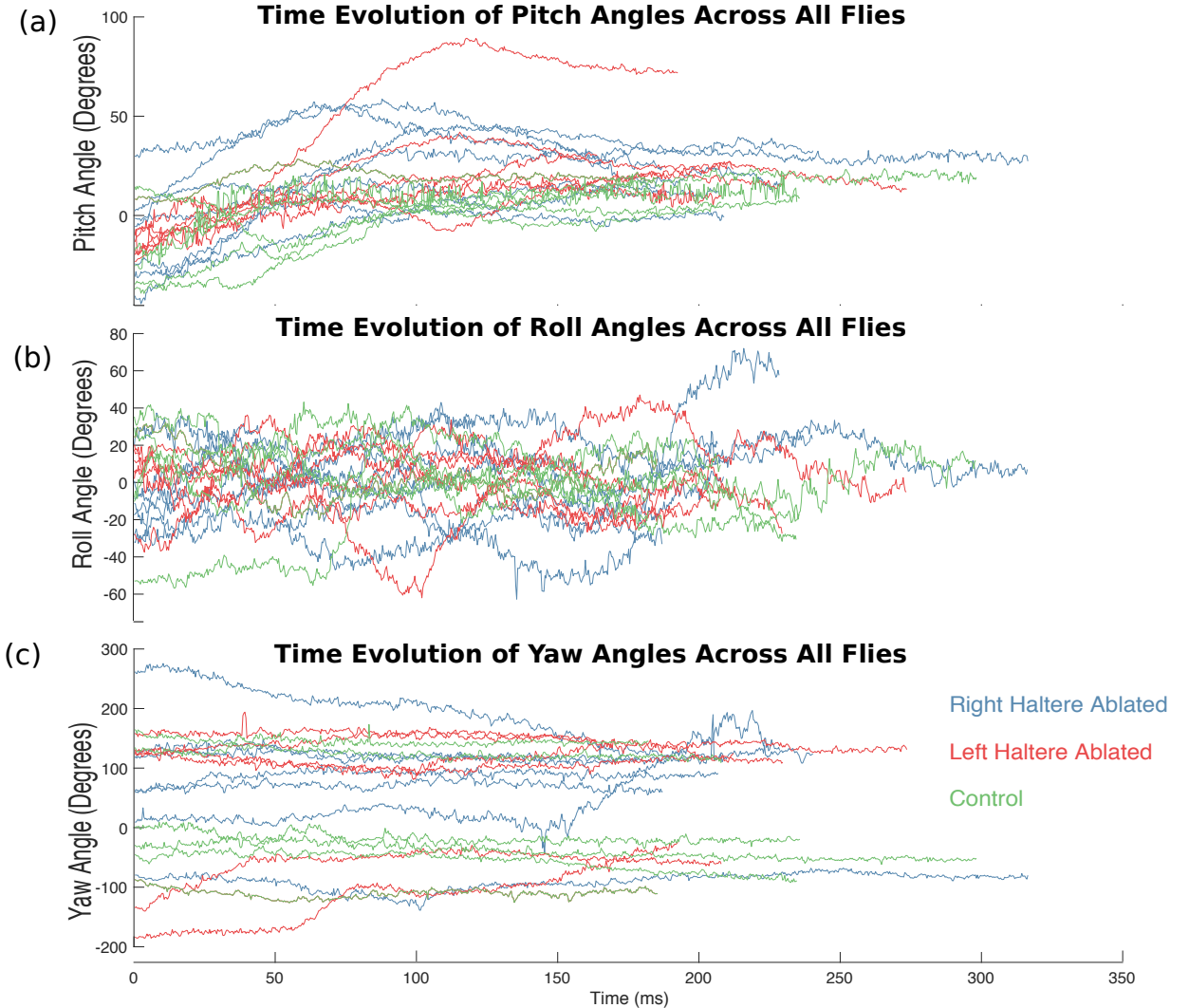


FIGURE 19: A plot showing the time evolution of (a): pitch, (b): roll and (c): yaw angles for all flies.

The time evolution plots of body angles show no segregation of body angles for a given treatment group. To quantify this, the angular velocities along each rotational axes were calculated. Each curve was smoothed using a moving average with a window length of 50. The mean

angular velocities were then compared across treatment groups (Figure 20). Statistical analyses show that the pitch velocity and the yaw velocity are not different across treatment groups (Pitch velocity: $p = 0.46$, Yaw Velocity: $p = 0.23$). But, roll velocity of the right haltere ablated flies is higher than that of control flies ($p = 0.03$), and the left haltere ablated flies ($p = 0.02$). A Wilcoxon ranksum test indicates that roll velocities of the left haltere ablated flies and control flies are not different ($p = 0.36$)

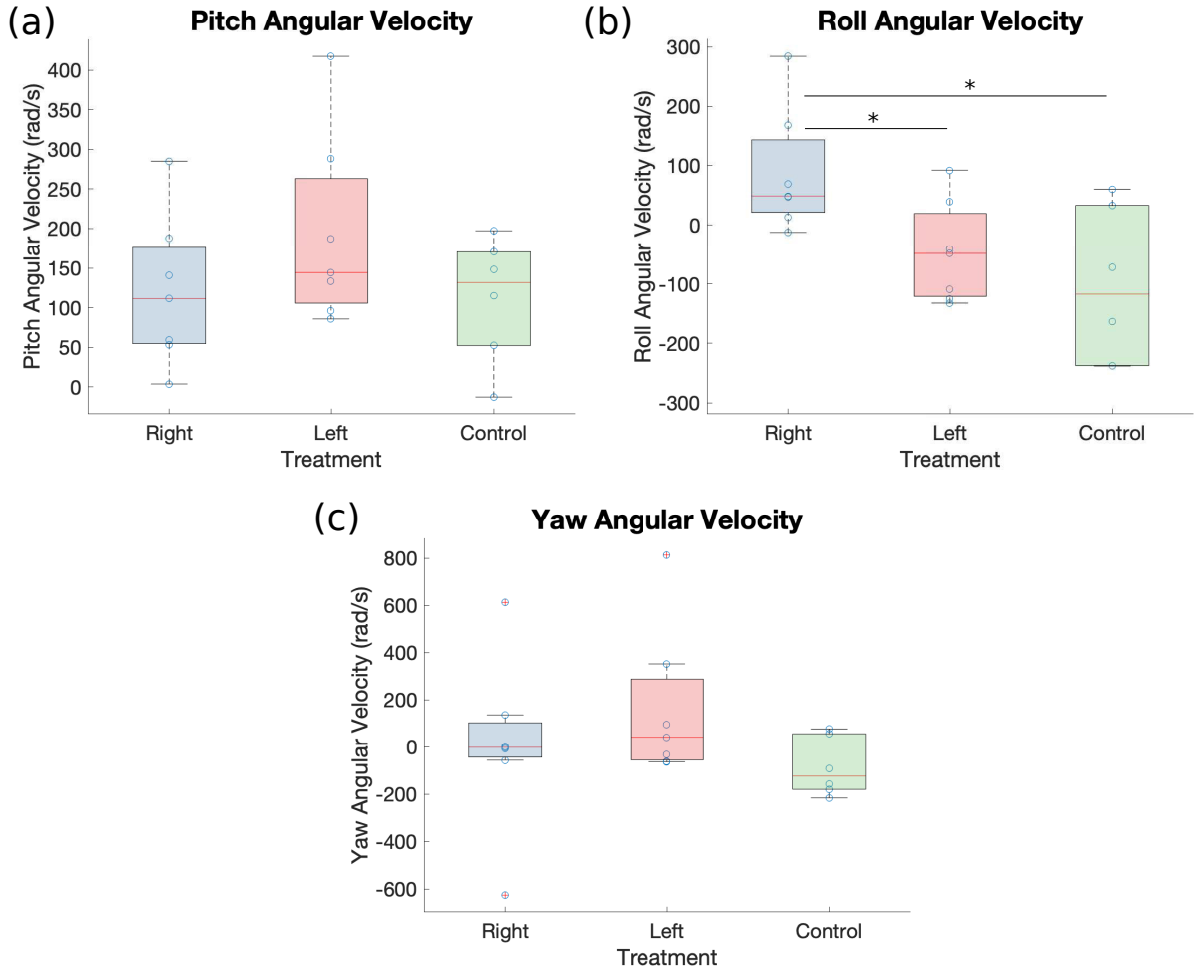


FIGURE 20: Comparing angular Velocities for, (a): Pitch, (b): Roll, (c): Yaw across treatment groups.

Comparing average body angles across treatments

Visual inspection of flight bout videos show that unilateral haltere ablated flies tend to have their bodies more vertical (higher pitch) than control flies during flight. To quantify this, the mean body angles were compared for the different treatment groups (Figure 21). Statistical tests confirmed that the mean pitch angle of left haltere ablated flies is higher than that of control flies ($p = 0.02$). The right haltere ablated flies are not statistically different in mean pitch than control flies ($p = 0.13$). No difference in the roll and yaw angles across treatments were suggested by a Kruskal Wallis test (Roll: $p = 0.71$, Yaw: $p = 0.60$).

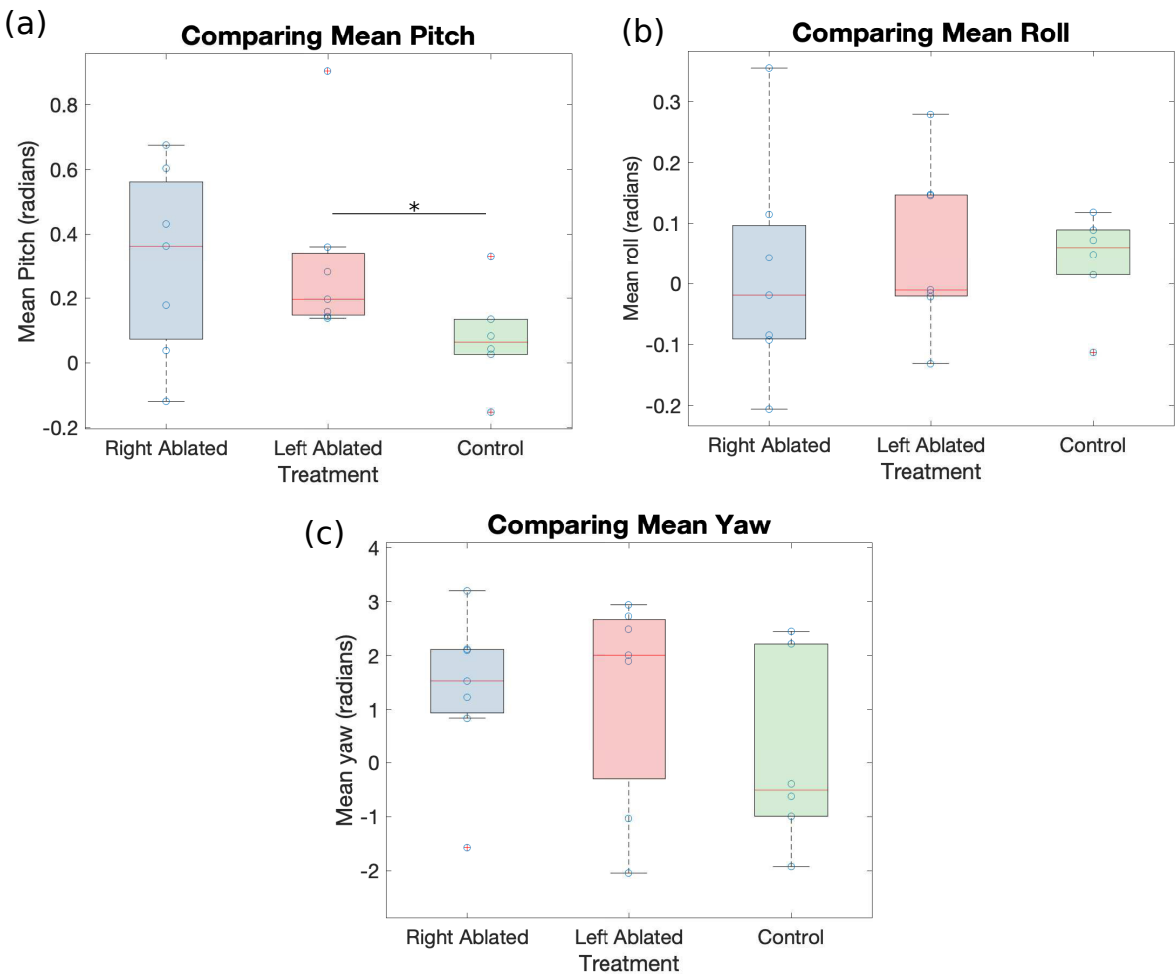


FIGURE 21: (a) Variation of mean pitch across treatment groups. The average pitch angle for left haltere ablated flies is higher than that of control flies. (b): Variation of mean roll across treatment groups. (c): Variation of mean yaw across treatment groups.

3.2.2 WING KINEMATIC PARAMETERS

For the three treatment groups of haltere ablations, dorsal excursion maxima, ventral excursion maxima, and peak to peak amplitudes were compared for each wing. The wing-wing differences in these parameters were also compared.

These are the wing kinetic parameters that modulate flight. Comparing these parameters across haltere ablation treatments might indicate how halteres affect flight.

Stroke Angles

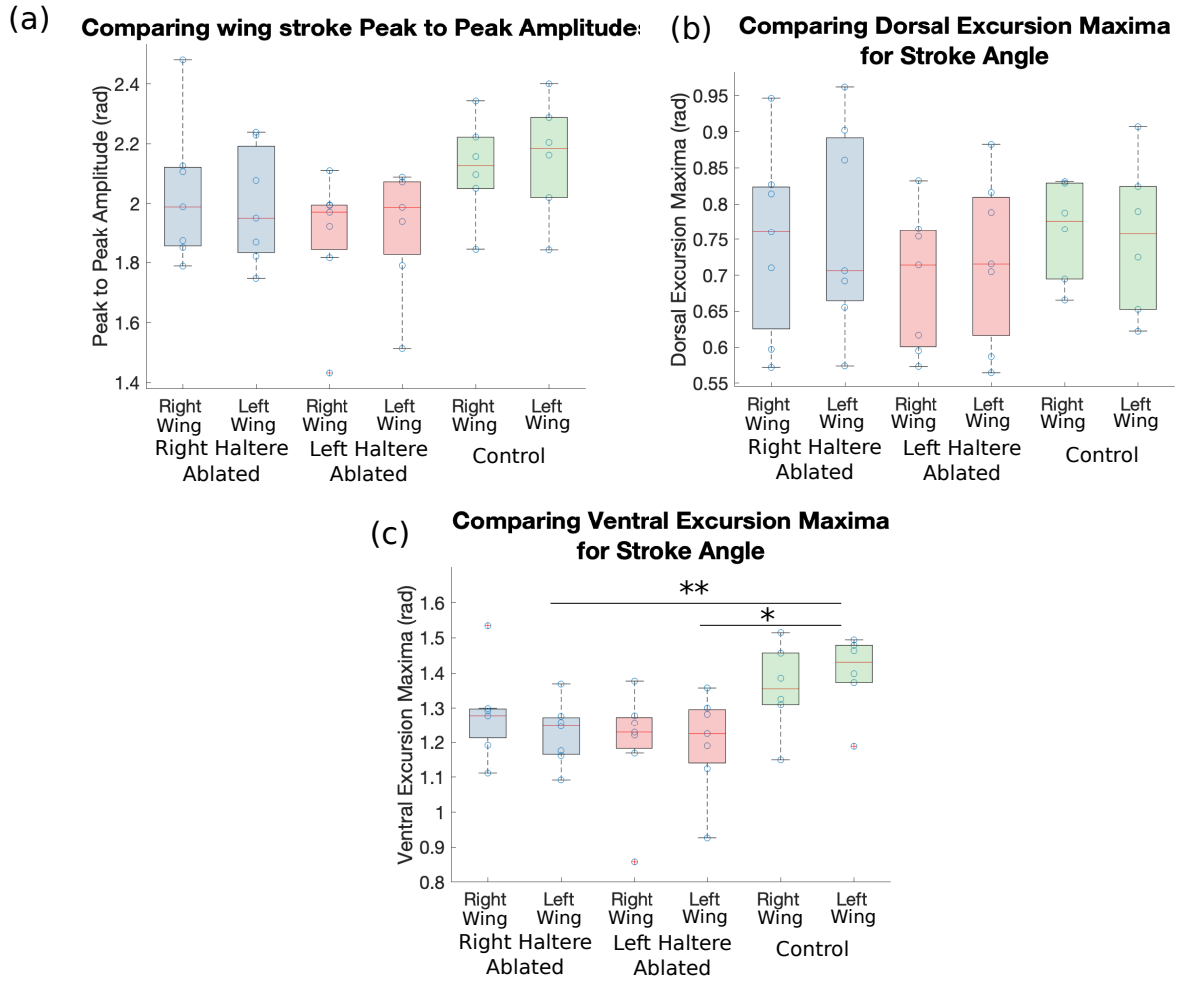


FIGURE 22: Comparing (a): peak to peak amplitudes, (b): Dorsal excursion maxima and (c): ventral excursion maxima for stroke angles across treatments and across wings. This plot shows the variation of parameters for each wing across treatments and across wings in individual treatment groups.

Left wing Ventral excursion maxima of flies in the control group is higher than that of flies in the left haltere ablated group ($p = 0.02$) and those in the right haltere ablate group ($p = 0.01$) (Figure 22). Unilateral haltere ablation reduced the ventral excursion maxima of the stroke angles. But, peak to peak amplitudes and dorsal excursion maxima do not vary across treatments for either wing. (Right Wing Stroke Amplitude: $p = 0.19$, Left Wing Stroke Amplitude: $p = 0.17$; Right Wing Dorsal Excursion Maxima: 0.54; Left Wing Dorsal Excursion Maxima: 0.80) The right wing ventral excursion maxima are not different across treatments ($p = 0.12$).

Statistical analysis also indicate no difference between right and left wing for the calculated parameters. The following table summarizes the comparison p values.

TABLE 2: Comparisons between right and left wings for stroke angle maxima

Treatment	Amplitude	Dorsal Maxima	Ventral Maxima
Control	0.81	0.81	0.48
Right Haltere Ablated	0.80	0.90	0.20
Left Haltere Ablated	0.80	0.81	1

Figure 23 compares the right wing - wing left differences for ampltiude, and dorsal and ventral maximas across treatment groups. Statistical analyses revealed no significant difference across treatments. (Amplitude: $p = 0.23$; Dorsal Excursion Maxima: $p = 0.71$; Ventral Excursion Maxima: $p = 0.14$)

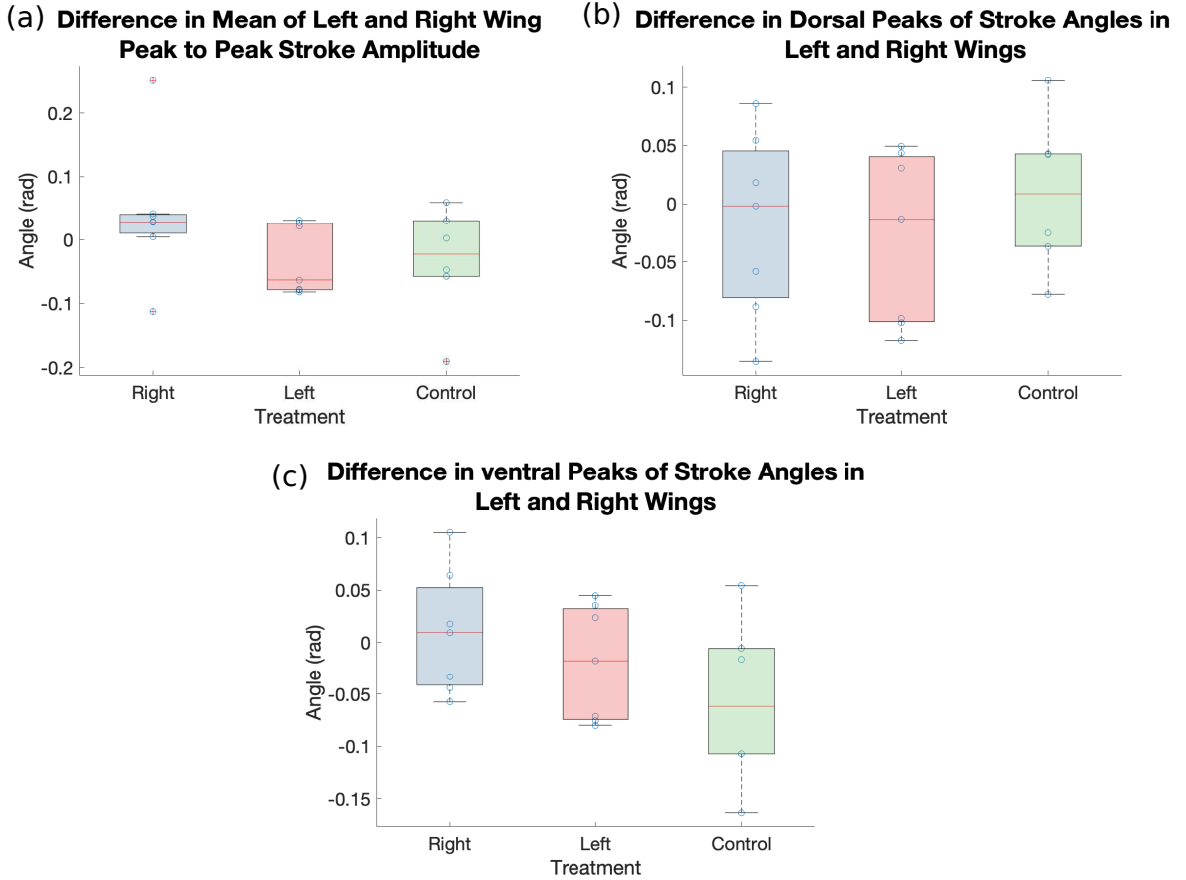


FIGURE 23: Comparing the difference of (a): Peak to Peak Amplitude, (b): Dorsal Excursion maxima, (c): Ventral Excursion maxima in stroke angles, between the left wing and right wing across the different treatment groups

Deviation Angles

Figure 24 compares the deviation angle maxima across treatment groups. Statistical tests revealed no significant differences between the wings across treatments, and between treatments across the right and left wing (Right Wing Deviation Amplitude: $p = 0.54$, Left Wing Deviation Amplitude: $p = 0.75$; Right Wing Dorsal Excursion Maxima: $p = 0.41$; Left Wing Dorsal Excursion Maxima: $p = 0.86$; Right Wing Ventral Excursion Maxima: $p = 0.27$; Left Wing Ventral Excursion Maxima: $p = 0.60$)

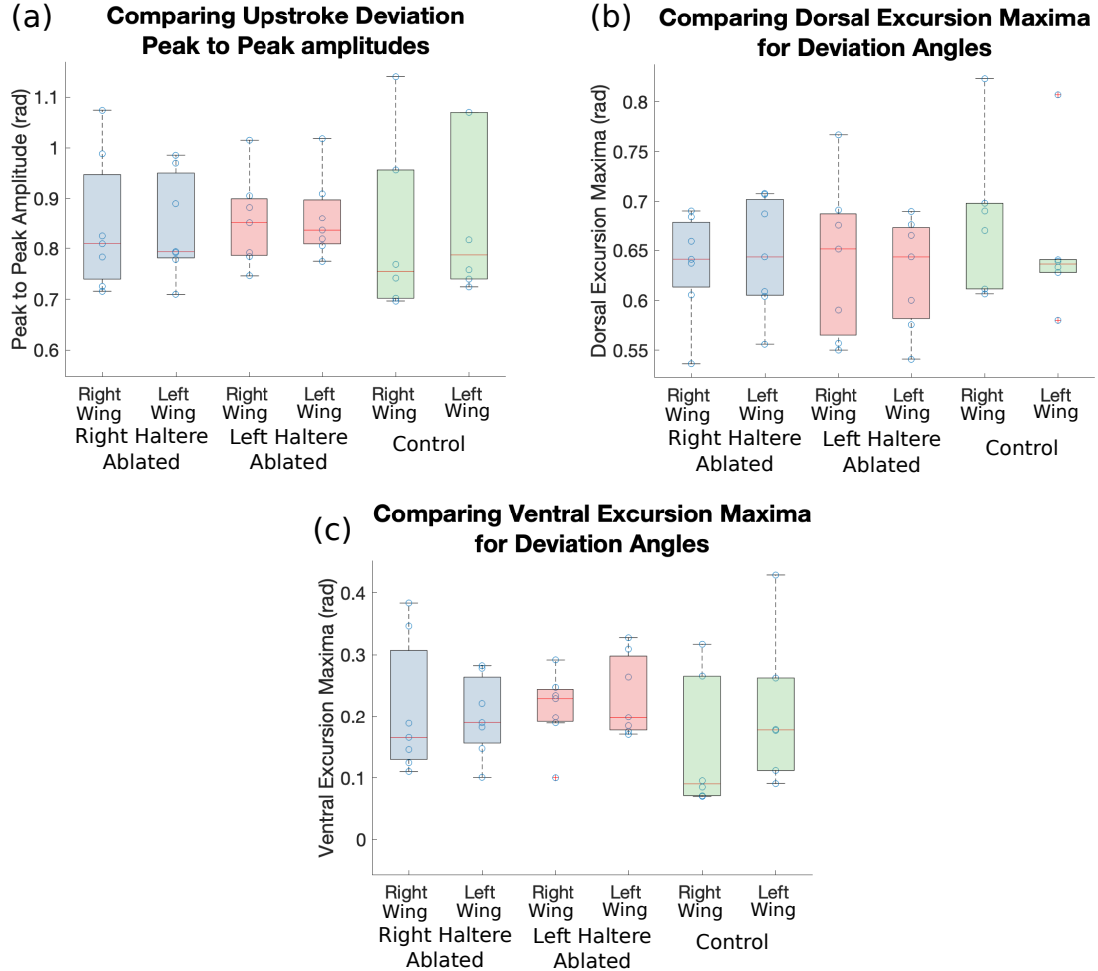


FIGURE 24: Comparing (a): peak to peak amplitudes, (b): Dorsal excursion maxima and (c): ventral excursion maxima for deviation angles across treatments and across wings. This plot shows the variation of parameters for each wing across treatments and across wings in individual treatment groups.

The following table has the statistical test results for comparisons between left and right wing for deviation angle maximas.

TABLE 3: Comparisons between right and left wings for deviation angle maxima

Treatment	Amplitude	Dorsal Maxima	Ventral Maxima
Control	0.69	0.48	0.31
Right Haltere Ablated	0.90	0.71	0.80
Left Haltere Ablated	0.80	0.80	0.90

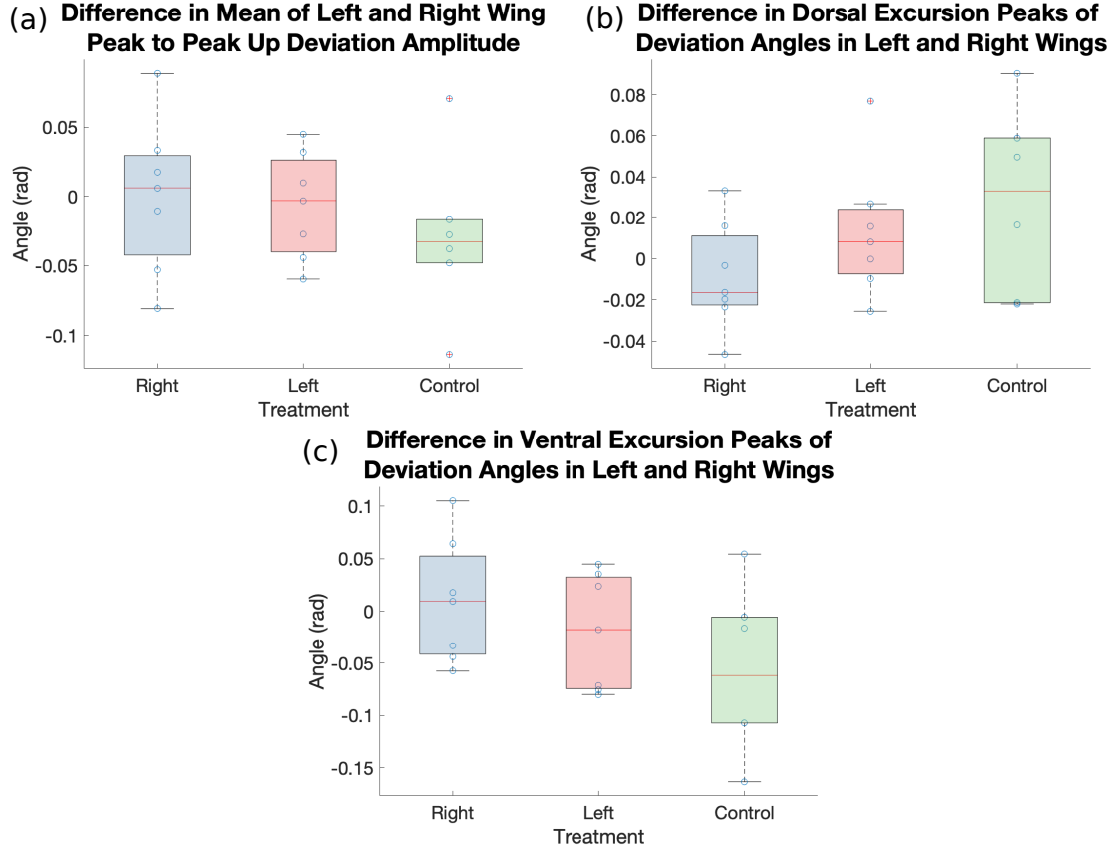


FIGURE 25: Comparing the difference of (a): Peak to Peak Amplitude, (b): Dorsal Excursion maxima, (c): Ventral Excursion maxima in deviation angles, between the left wing and right wing across the different treatment groups.

Figure 25 shows the right wing - left wing differences across treatment groups. Statistical analyses indicate no difference across the treatments (Amplitude: $p = 0.55$; Dorsal Excursion Maxima: $p = 0.28$; Ventral Excursion Maxima: $p = 0.31$)

It must be noted that the variance in the measured parameters is high and therefore, conclusions made from statistical indications may not necessarily be true.

CHAPTER 4

DISCUSSION

4.1 HALTERE ABLATED FLIES PITCH UP

Left haltere ablated flies have a higher average angle of pitch during flight in the first 20 wingbeats than control flies (Figure 21).

As the fly flaps its wings, there is an angular momentum associated with the movement. The direction of this angular momentum is almost perpendicular to the stroke plane. In absence of mechanosensory feedback for control of flight, the fly has to rely on visual inputs and passive stability to maintain control. One way to keep stable would be to align the direction of angular momentum with the most significant torque acting on the body, to minimize rotations. It is likely that pitching up provides such an alignment. But, it is unclear whether flies actively perform this manoeuvre for stability, or if the pitch variation is passively induced due to lack of feedback.

If this were true, it is not efficient for a fly to fly in such a position to maintain flight control, without relying on mechanosensory modalities. Having a higher pitch angle while translating forward in flight would result in a lot more drag resistance, resulting in the fly spending a lot more energy, reducing the range and speed of flight.

4.2 RIGHT HALTERE ABLATED FLIES HAVE HIGHER ROLL VELOCITIES

Right Haltere ablated flies have higher roll velocities than control and left haltere ablated flies (Figure 20). This is interesting, considering that the time course of roll angles (Figure 19) does

not seem to indicate any difference in perturbations. Figure 20-(b) indicates that the median roll velocity for right haltere ablated flies is around 40 rad s^{-1} .

This result indicates that there is some degree of loss of control of flight in the roll axis in absence of the right haltere.

4.3 VENTRAL EXCURSION MAXIMA IN STROKE ANGLE IS REDUCED ON HALTERE ABLATION

The ventral excursion maxima in stroke angles for the left wing is reduced by almost 15% on unilateral haltere ablation (Figure 22).

Our results show wing inhibition on unilateral haltere ablation. This result is supported in part by tethered flight experiments in *Drosophila*, which showed that unilateral haltere ablation attenuated the response of the ipsilateral wing (Dickinson 1999). Interestingly, this result directly conflicts with the free flight experiments in *Musca*.

This particular results casts doubt on our hypothesis of haltere inputs inhibiting ipsilateral wingstroke amplitude. It is important to note in parallel that the ventral excursion does not translate to peak to peak amplitudes, although the two are dependent variables. A closer look at the analysed data indicates high variance in many parameters, suggesting that a sample size of 7 may be insufficient. Data was collected for a higher sample size of 15, and the results of this complete analysis could provide more conclusive results about the trends of wing kinetic parameters and body angles.

The trend is not evident for the stroke angles in the right wing ($p = 0.11$), but it is likely that this is an effect of a low sample size.

4.4 COMPARISONS WITH FREE FLIGHT IN HALTERE ABLATED *Musca*

One of the motivations for conducting this project came from the results of free flight experiments in *Musca* (Sujay Balebail, Vardhanam Daga, Sanjay Sane, *unpublished*), which indicated

that unilaterally haltere ablated flies show increase in ipsilateral wing stroke amplitude. Hence, a right haltere ablated fly would increase its right wing amplitude and roll to the left.

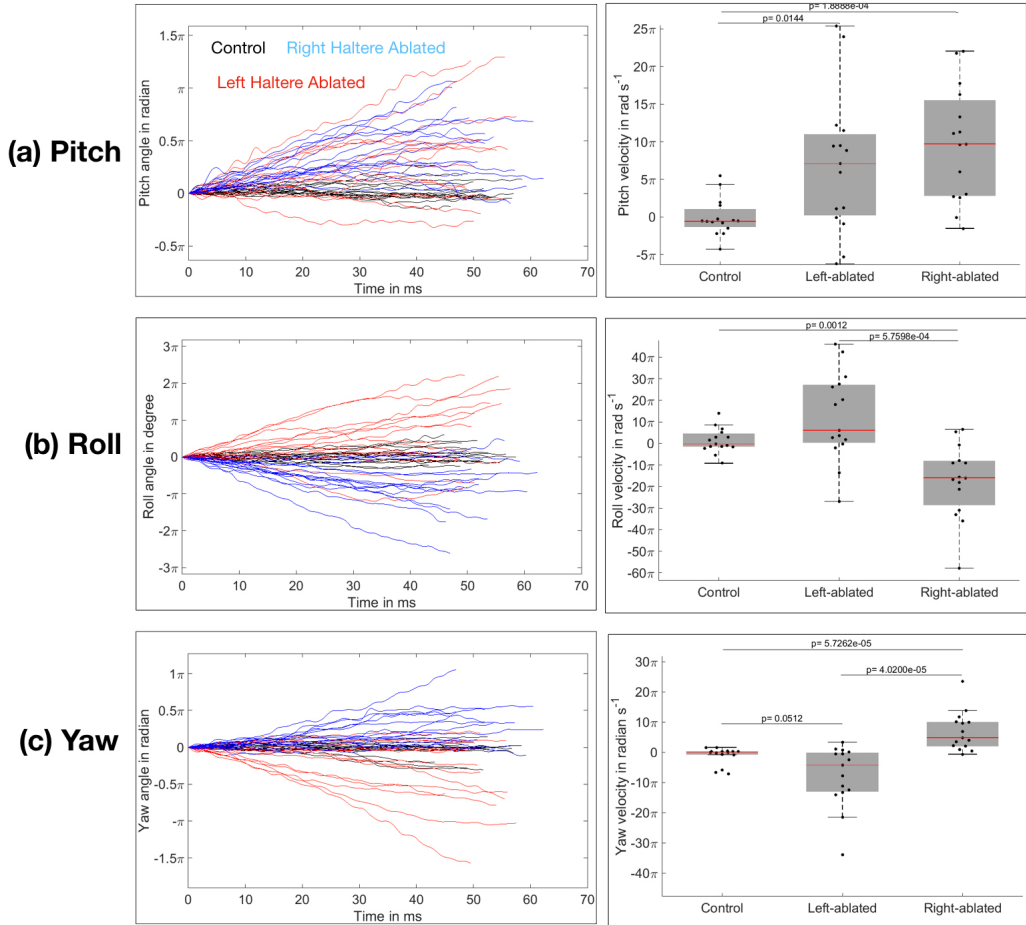


FIGURE 26: Free flight study in *Musca* show that unilateral haltere ablated flies have an handedness in (b): roll and (c): yaw rotation. (a): Haltere ablated flies tend to pitch up. (Image from Sujay Balebail)

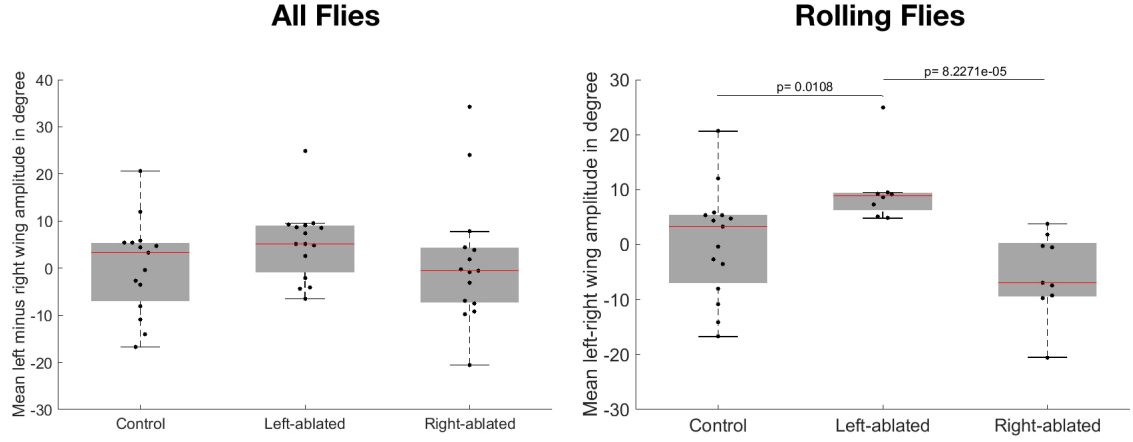


FIGURE 27: Free flight study in *Musca*: Unilateral haltere ablation **increases** ipsilateral wingstroke amplitude. The effect is more stark in flies that roll. (Image from Sujay Balebail)

Soldier flies do not exhibit handedness in rotations with haltere ablation, and there is no statistically detectable difference in the wing-wing amplitude difference. It is interesting that our experiments in soldier flies do not support the trends observed for haltere ablated free flight in *Musca*. To understand the differences in the trends it is relevant to discuss the differences in our experiments and those in *Musca*.

Setup

- *Lighting*

Experiments in soldier flies were done in a well lit room, with a lot of ambient natural light. On the other hand, the experiments in *Musca* was conducted in a windowless room, with halogen lamps and a UV lamp as the only other light sources. Hence, visual feedback received by soldier flies and *Musca* in their respective setups were very different.

- *Perch for takeoff*

In the *Musca* experiment, a frustum created using a falcon with its tip cut-off, was used as a perch. Flies were collected in a container with this frustum attached to the cap. Flies would climb to the tip of the frustum and take off. On the other hand, in our experiment with soldier flies, the perch is a horizontal ice-cream stick placed at the mouth of the falcon. The flies would walk up to the stick and take off.

Different perches could result in different initial perturbations that a fly experiences as it takes off. These initial perturbations play an important role in the flight attitude of the fly, especially if we are measuring the time course of perturbations in flight.

- *Haltere Ablations*

Haltere ablations in my experiments involved complete removal of the haltere, from the base. Experiments in *Musca* only removed the bulb, keeping the stalk intact. For the case of *Musca*, the sensory fields are intact, but no forces can be relayed by them. Hence, it can be assumed that there are **no** haltere inputs. In our experiments in soldier flies, ablation involves removal of the sensory fields too. Any information relayed to the fly from the haltere nerve in this case would be random noise. Random noise as haltere inputs should result in more erratic behavioural outputs that can be characterised for better understanding of the role of haltere inputs on flight control.

Fly Physiology

- *Wingbeat Frequency*

The average wingbeat frequency in *Musca* is around 200 Hz (World Book Encyclopedia, Chicago 1997). Soldier flies average at around 120 Hz. From the perspective of timescale, one wingbeat in *Musca* takes 5 ms, and one wingbeat in soldier flies around 8.3ms.

Soldier flies have more time to integrate information from other sensory modalities and perhaps, execute better control of flight. Visual input integration takes around 25-30ms (Yarger, 2016). This extra time for sensory integration could be why unilateral haltere ablated soldier flies do not exhibit rotational instability, whereas unilaterally haltere ablated *Musca* do.

- *Passive Stability*

The structure of the fly body also plays a role in stability against rotations. The higher the moment of inertia about an axis, the lower the tendency to rotate about that axis. Soldier flies have longer, sleeker bodies than *Musca*. Hence, the moment of inertia about the pitch, roll and yaw axes is higher for soldier flies than in *Musca*.

It is important to note here that complete loss of control in flight was observed in soldier

flies with bilateral haltere ablation. Hence, associating control of flight in unilateral haltere ablated flies with purely passive stability is not accurate.

H. illucens also have longer wings than *Musca*. This could also correlate to more campaniform sensillae on the wings of soldier flies. Hence, soldier flies could be relying on mechanosensory feedback from these sensillae to compensate for lack of haltere inputs. Obviously, these are alone not enough to maintain stable flight, but considering the timescales of sensory integration, it is a possible mechanism for maintaining flight control in unilaterally haltere ablated flies, a system with limited feedback.

For complete characterisation of the role of halteres in flight, it is pertinent to study halteres in free flight. Soldier flies, with their long halteres that can be filmed easily in flight are a promising model for understanding the role on halteres in flight control. Our results show that soldier flies are generally stable in flight, even with unilateral haltere ablation. If visual feedback plays a more important role than passive stability to explain our results, then soldier flies can be used in dimly lit flight chambers for studies on the role of haltere in flight control.

4.5 DIGITIZATION AND DEEPLABCUT

One of the major challenges in this project was digitization of 3D coordinates from videos. A deep learning tool, DeepLabCut has been used for aiding in digitization. This tool had not been used in our research group before. I helped in setting up the protocol for using DeepLabCut on the computational cluster at NCBS. I also interfaced DeepLabCut (Mathis et al. 2018) and the data viewer DLTdv7 (Hedrick et al. 2008) which allows for 3D calibration aided manual digitization. This interfacing allows for improved accuracy and precision of the manually labeled dataset required for training the neural network.

DeepLabCut reduces manual effort required in digitisation greatly and now that it has been established in the lab, it will be used for many other projects. Currently it is being used in the lab for characterising initiation of flight via the tarsal reflex.

4.6 FUTURE DIRECTIONS

4.6.1 FROM THE CURRENT DATASET

The data analysed in this project is a very small fraction of the filmed flight bouts. The collected dataset has three flight bouts per fly before and after treatment, for 15 flies in 4 treatment groups; control, left haltere ablated, right haltere ablated and bilateral haltere ablation. The first step would be to complete the analysis of all the collected flight bouts.

In my analysis, I have only considered two wing kinetic parameters: stroke angle and deviation angle. Measuring wing rotation angle requires digitisation of an additional point on the wing, to define a wing chord. Manually identifying the point required for defining the wing chord accurately is difficult, but possible. The wing rotation angles can be obtained from collected videos, but doing so requires more sophistication in implementing the DeepLearning tool, or requires significantly more time to do so manually.

Not all flies take off from the top of the falcon or from the ice cream stick in our behavioural rig (Figure 12). Some flies climb out and take off from the side of the falcon. Some flies take off from the top of the falcon, but facing in the opposite direction to the eventual flight trajectory. These take off perches play a role in defining the initial perturbations in flight. It is important to detach the effects of these on flight attitude. The outputs of complexities in the environment should not be mistaken for complexities in the behaviour.

The current dataset only has flies that initiated flight from the ice cream stick, or from top of the falcon.

4.6.2 DISSOCIATING THE EFFECTS OF VISUAL INPUT ON FLIGHT CONTROL

Visual feedback is one of the possible reasons for stability of flight in unilateral haltere ablated soldier flies, considering our results and the results of the experiments in *Musca*. To confirm this, free flight of haltere ablated flies in a dimly lit flight arena can be compared to the the collected data.

If flies maintain stable, controlled flight in a dimly lit arena even after haltere ablation, it

is likely that the visual inputs play a significant role in maintaining flight stability in our experiments. If so, soldierflies can be used in dimly lit flight arenas for further free flight experiments to study the role of halteres in flight.

4.6.3 FURTHER EXPERIMENTS IN FREE FLIGHT

Complete understanding of the role of halteres in Dipterans requires a lot more characterization in free flight. The following are a few studies that can be done with soldier flies in free flight for a clearer understanding off the role of halteres in flight.

Establish trajectory of haltere movement in flight

Current information on the movement of halteres come from tethered flight experiments and simulations (Thompson et al. 2009). The trajectory of halteres have been a basis for understanding how rotational instabilities can be sensed by the sensory fields at the base of the haltere. To my knowledge, no studies have identified haltere trajectories in free flight. Soldier flies, having long visible halteres could be a great model system for such a study. With high speed filming and precise calibration methods, obtaining trajectories of soldier fly halteres in free flight is a study waiting to happen. The trajectories of halteres in free flight, especially as the fly performs manoeuvres like banking, pitching or rolling would provide better insight into the forces experienced by the haltere and the possible role of individual sensory fields.

Halteres and Saccades in Free Flight

Tethered flight studies in *Drosophila* have indicated that haltere inputs are necessary for performing voluntary saccades (Bender et al. 2006). When a fly performs a voluntary saccade, it has to inhibit the haltere reflex loop (Chan et al. 1998). L shaped boxes can be used for studying turning in flight; voluntary pitch rotations if placed vertically, or a combination of yaw and roll rotations if placed horizontally. Studying a fly's flight pattern in such a system, in absence of halteres could provide information on the haltere reflex loop and its inhibition for maintaining control during voluntary saccades.

4.7 REFERENCES

1. Bender JA, Dickinson MH (2006) Visual stimulation of saccades in magnetically tethered *Drosophila*. *J Exp Biol* 209:3170–3182
2. Chan, W.P., Prete, F., and Dickinson, M.H. (1998) Visual input to the efferent control system of a fly's 'gyroscope'. *Science*, 289, 289-292.
3. Dickinson MH. (1999). Haltere-mediated equilibrium reflexes of the fruit fly, *Drosophila melanogaster*. *Philos Trans R Soc Lond B Biol Sci* 354:903–16.
4. Hedrick, T. L., Software techniques for two- and three-dimensional kinematic measurements of biological and biomimetic systems, *Bioinspiration and Biomimetics*, 2008
5. Mathis, Alexander, Pranav Mamidanna, Kevin M. Cury, Taiga Abe, Venkatesh N. Murthy, Mackenzie Weygandt Mathis and Matthias Bethge. “DeepLabCut: markerless pose estimation of user-defined body parts with deep learning.” *Nature Neuroscience* 21 (2018): 1281-1289.
6. Thompson, R.A., Wehling, M.F., Evers, J., and Dixon, W.E. (2008). Body rate decoupling using haltere mid-stroke measurements for inertial flight stabilization in Diptera. *Journal of Comparative Physiology A*, 195, 99-112.